AD-A015 129

WATER TUNNEL SIMULATION STUDY OF THE LATER STAGES OF WATER ENTRY OF CONICAL HEAD BODIES

J. H. Kim, et al

Pennsylvania State University

Prepared for:

Naval Sea Systems Command

18 June 1975

DISTRIBUTED BY:

NTIS

National Technical Information Service
U. S. DEPARTMENT OF COMMERCE

279179

AD A015129

WATER TUNNEL SIMULATION STUDY OF THE LATER STAGES OF WATER ENTRY OF CONICAL HEAD BODIES

J. H. Kim and J. W. Holl

Technical Memorandum
File No. TM 75-177
June 18, 1975
Contract No. N00017-73-C-1418

Copy No. 13

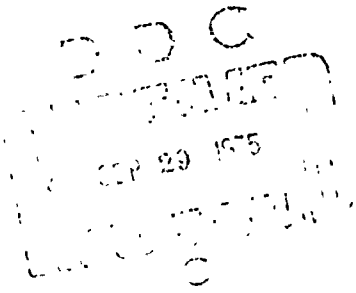

The Pennsylvania State University
Institute for Science and Engineering
APPLIED RESEARCH LABORATORY
Post Office Box 30
State College, PA 16801

APPROVED FOR PUBLIC RELEASE
DISTRIBUTION UNLIMITED

Reproduced by
NATIONAL TECHNICAL
INFORMATION SERVICE
US Department of Commerce
Springfield VA 22151

NAVY DEPARTMENT

NAVAL SEA SYSTEMS COMMAND

UNCLASSIFIED

SECURITY CLASSIFICATION OF THIS PAGE (When Data Entered)

REPORT DOCUMENTATION PAGE		READ INSTRUCTIONS BEFORE COMPLETING FORM
1. REPORT NUMBER TM 75-177	2. GOVT ACCESSION NO.	3. RECIPIENT'S CATALOG NUMBER
4. TITLE (and Subtitle) WATER TUNNEL SIMULATION STUDY OF THE LATER STAGES OF WATER ENTRY OF CONICAL HEAD BODIES		5. TYPE OF REPORT & PERIOD COVERED Technical Memorandum 6. PERFORMING ORG. REPORT NUMBER
7. AUTHOR(s) J. H. Kim and J. W. Holl		8. CONTRACT OR GRANT NUMBER(s) N00017-73-C-1418
9. PERFORMING ORGANIZATION NAME AND ADDRESS Applied Research Laboratory P. O. Box 30 State College, PA 16801		10. PROGRAM ELEMENT, PROJECT, TASK AREA & WORK UNIT NUMBERS
11. CONTROLLING OFFICE NAME AND ADDRESS Naval Sea Systems Command Washington, DC 20362		12. REPORT DATE June 18, 1975 13. NUMBER OF PAGES 71
14. MONITORING AGENCY NAME & ADDRESS(if different from Controlling Office)		15. SECURITY CLASS. (of this report) UNCLASSIFIED 15a. DECLASSIFICATION/DOWNGRADING SCHEDULE

16. DISTRIBUTION STATEMENT (of this Report)

Approved for public release. Distribution unlimited.
Per NAVSEA - September 10, 1975.

17. DISTRIBUTION STATEMENT (of the abstract entered in Block 20, if different from Report)

18. SUPPLEMENTARY NOTES

19. KEY WORDS (Continue on reverse side if necessary and identify by block number)

AIR FLOW COEFFICIENT
CAVITATION COEFFICIENT
CAVITY RUNNING
CONICAL HEAD
SIMULATION
VAPOROUS CAVITIES
WATER ENTRY

20. ABSTRACT (Continue on reverse side if necessary and identify by block number)

The feasibility of utilizing a water tunnel for studying the cavity-running phase of water entry was explored in thi test program. Using conical head models, steady state ventilated cavity tests were conducted in the 12-inch water tunnel to determine cavitation number versus cavity length, pressure distribution, ventilation air flow coefficient and cavity area coefficient. The cavitation number versus cavity length and pressure distribution data were found to be in excellent agreement with existing data for vaporous cavities,

DD FORM 1 JAN 73 1473 EDITION OF 1 NOV 65 IS OBSOLETE

UNCLASSIFIED

SECURITY CLASSIFICATION OF THIS PAGE (When Data Entered)

while the ventilation air flow coefficient showed qualitative trends which were similar to those for ogive bodies. Following these steady-state tests, a cavity attrition test was performed to simulate the decay of the cavity in the last stage of water entry prior to fully wetted flow. This test was performed by observing the cavity decay following cut-off of tunnel power and it was found that the deceleration was approximately 3 ft/sec^2. The instantaneous cavitation number versus the instantaneous cavity length was found to be in good agreement with the steady-state data. This can be interpreted as an indication that quasi-steady analysis may be useful for studying water entry phenomenon at least for decelerations of the order of 3 ft/sec^2.

Abstract: The feasibility of utilizing a water tunnel for studying the cavity-running phase of water entry was explored in this test program. Using conical head models, steady state ventilated cavity tests were conducted in the 12-inch water tunnel to determine cavitation number versus cavity length, pressure distribution, ventilation air flow coefficient and cavity area coefficient. The cavitation number versus cavity length and pressure distribution data were found to be in excellent agreement with existing data for vaporous cavities, while the ventilation air flow coefficient showed qualitative trends which were similar to those for ogive bodies. Following these steady-state tests, a cavity attrition test was performed to simulate the decay of the cavity in the last stage of water entry prior to fully wetted flow. This test was performed by observing the cavity decay following cut-off of tunnel power and it was found that the deceleration was approximately 3 ft/sec^2. The instantaneous cavitation number versus the instantaneous cavity length was found to be in good agreement with the steady-state data. This can be interpreted as an indication that quasi-steady analysis may be useful for studying water entry phenomenon at least for decelerations of the order of 3 ft/sec^2.

TABLE OF CONTENTS

[1] INTRODUCTION

Water entry is a phenomenon associated with the passage of a body from a gaseous environment into a liquid medium. Its importance has been well recognized due to the fact that the performance of a body such as a missile entering the water is irrevocably influenced by cavity formation behind it. In a water entry, seemingly small factors of various kinds such as gas flows within the cavity, physical properties of the liquid (surface tension, dissolved gas nuclei, etc.), and even the surface of the missile can greatly affect the cavity behavior and hence the whole behavior of the object [Waugh and Stubstad (1972)].

When an airborne missile impacts on the water, it creates a splash of water along the body surface, eventually forming a closed cavity as the body submerges beneath the free surface. As the missile travels along its trajectory in the water, the cavity becomes gradually elongated, and at a later stage it pinches off into two cavities. Subsequent to this so-called "deep closure", a nearly steady state condition prevails for a short while before the cavity starts to abate and finally collapses as the velocity of the missile decreases while the ambient hydrostatic pressure increases.

The early stages of the water entry cavity have been investigated by May (1972), Baldwin (1972), and Aronson et. al (1974 a, b). Yet, comparatively little has been studied about the later stages of the cavity running, its collapse and dispersal, although these later phases may be suited for investigation in the water tunnel.

The conventional and straightforward measurements of the water

entry phenomena are known to require a large instrumented facility and are time consuming. Measurements are usually done in a hydroballistics tank by shooting the test objects into the water. Clearly, this kind of test condition will most closely resemble the actual situation. On the other hand, it is admittedly time consuming, especially when it is desired to repeat the same test conditions many times to reproduce the data points.

The present study was motivated by a desire to explore the possibility of utilizing a water tunnel in investigating this kind of phenomenon. It is obvious that the water tunnel cannot be used in observing the early stages of a water entry including the splash and pinching off of the cavity, but a reasonable simulation of the later stages of the phenomena may be possible.

As a first step in this program, steady state measurements of the cavitation number, cavity length, the ventilation air flow coefficient, cavity area coefficient, and pressure distribution were made on conical head bodies for ventilated cavities. In addition, an exploratory investigation was conducted of the cavity decay process by establishing a cavity and then observing the cavity after the water tunnel power was turned off. The steady state data may be useful in analyzing the unsteady instantaneous data obtained by photographic measurements of the cavity attrition.

[2] DESCRIPTION OF THE EXPERIMENTS

All the tests were conducted in the 12-inch water tunnel of the Garfield Thomas Water Tunnel Building at the Pennsylvania State

University.

Models used for the tests were:

Model I --- 45° apex angle conical head joined to 1/2" diameter cylindrical afterbody (ARL Drawing No. SKB73162)

Model II --- 45° apex angle conical head joined to 1" diameter cylindrical afterbody (ARL Drawing No. SKB73158, and also Sketch Drawing No. SKC73159 for pressure coefficient measurements)

Model III --- 18° apex angle conical head joined to 1/2" diameter cylindrical afterbody (ARL Drawing No. SKB73162)

Model IV --- 18° apex angle conical head joined to 1" diameter cylindrical afterbody (ARL Drawing No. SKB73156)

The geometrical advantages of using conical shaped head forms are briefly discussed by Baldwin (1972). In addition to these geometrical advantages, the steady state ventilated cavity measurements with these models can be compared with the earlier data of Rouse and McNown (1948) for vaporous cavities.

The experimental set-up for steady state measurements is illustrated in Figure 1.

Tests were conducted at velocities of 30, 45, and 50 ft/sec. The flow velocity was set by maintaining the manometer reading at a precalculated value. Then the air flow rate control valve was opened to

enable the formation of a ventilated cavity. It was then possible to measure the cavity length, the ventilation air flow rate, cavitation number, etc. The transducer registered either P_∞ or P_c by a flip of the switch in either direction.

For the pressure distribution measurement, a 45° apex angle conical head joined to 1 inch diameter cylindrical afterbody [Model II] with nine pressure taps along the body surface was used. For this particular test, the transducer was connected to a multi-channel scani-valve which relayed each of the pressures individually to the transducer. The test set-up would be essentially the same as Figure 1 with the addition of a scani-valve.

The models were marked at every half inch from the edge of the cone base so that the cavity length could be visually controlled at a desired length. The ventilation air was introduced through the six holes located along the periphery of the cylindrical afterbody slightly behind the base of the conical head.

The cavity attrition test set-up is illustrated in Figure 2. The test sequence was as follows:

(1) First, a steady state cavity was established. A ventilated cavity was used since in the real water entry situation air rather than vapor is trapped inside the cavity.

(2) Then, the air flow was suddenly cut off. At the same time, the tunnel was shut down by a switch which also automatically flashed the strobe-light. This strobe-light flash was used for identifying the frame of the movie film which in turn

showed the exact moment the tunnel switch was shut off.

(3) During the aforementioned steps, the movie camera and the oscillogram continuously recorded the cavity length and the pressure history, with various pressures being measured by three transducers. Transducer No. 1 registered the cavity pressure P_c, transducer No. 2 registered $P_o - P_\infty$, while transducer No. 3 gave the free stream pressure, P_∞. The oscillogram gave a trace for the pressures so that one could later find instantaneous values for the pressures. After the test, the movie camera film was compared with the pressure traces. The instant of tunnel shut-down was recorded on both the movie camera (by the flash of a strobe-light) and the oscillogram. Since the camera film speed is known, it was possible to match the instantaneous pressures on the oscillogram with the instantaneous cavity length recorded on the movie camera film. Thus the plot of the instantaneous cavity length was obtained.

Typical steady state ventilated cavities for a 45° conical model and an 18° conical model are shown in Figures 3 and 4.

[3] TEST RESULTS AND DISCUSSION

3.1 Cavity Length and Cavitation Number

Figures 5 - 8 show the cavitation number versus dimensionless cavity length, L/D. The cavitation number σ is defined by

$$\sigma = \frac{P_\infty - P_c}{\frac{1}{2}\rho V_\infty^2} \qquad (1)$$

where P_∞ is the pressure at infinity, P_c is the pressure inside the cavity, and V_∞ is the upstream velocity. Some of the data obtained earlier by Rouse and McNown (1948) for a vaporous cavity are also plotted in Figure 8. The agreement between the two sets of data is excellent.

In all the observations, the cavity did not appear to start at the edge of the cone base but rather it detached from slightly behind the edge. This tendency is also in agreement with the observations of Rouse and McNown.

Figure 9 shows the same set of data as those of Figures 5 - 8 with cavity length normalized with respect to the maximum cavity diameter D_M. In Figure 10, cavity length is taken as twice the distance between the cone base and the position where the cavity diameter becomes maximum. In both Figures 9 and 10, cavitation number is seen to become nearly independent of the body shapes as cavity length increases but is strongly influenced by the body shapes for short cavities. The quantities L_M and D_M were measured from the photographs.

An attempt was made to find a universal curve (independent of cone angle) for cavitation number versus cavity length by normalizing the cavitation number with the desinent cavitation number corresponding to each model, but the result thus obtained was not satisfactory.

3.2 Ventilation Air Flow Coefficient

The ventilation air flow coefficient was measured over a range of flow conditions and is defined

$$C_Q = \frac{Q}{V_\infty D^2} \tag{2}$$

where Q is the flow rate of the air blown into the cavity, V_∞ is the upstream velocity and D is the model diameter.

In order to eliminate the possible effects of diffusion on the the air entrainment, it was necessary to ensure that the air pressure in the cavity be maintained at the same value as the saturation pressure of the dissolved gas in the free stream which is given by Henry's law, namely,

$$P_{G_S} = \alpha\beta \tag{3}$$

where α is the air content in the free stream in ppm and β is the Henry's law constant

Since we must have $P_c = P_{G_S}$ to assure no diffusion, this implies that we should have

$$P_\infty = \frac{1}{2}\rho V_\infty^2 \sigma + P_{G_S} \tag{4}$$

P_{G_S} can be obtained by measuring the air content α using the Van slyke apparatus. It is apparent that diffusion cannot be entirely eliminated by this procedure since the cavity pressure is not precisely constant throughout the cavity. σ is known as a function of L/D from the

previous measurements. Therefore, for a prescribed value of L/D or σ, one can choose P_∞ according to Equation (4) so that diffusion across the cavity wall will be minimized. However, since the air was continuously forced into the tunnel during the test, the air content α likewise varied and so it was necessary to readjust the value of P_∞ in order to satisfy Equation (4) and thereby minimize diffusion.

In addition to minimizing the effects of diffusion on C_Q it was also important to eliminate vaporous cavitation. This was accomplished by operating the facility at sufficiently high pressures.

The information for the ventilation air flow coefficient can serve a useful purpose in studying either the air entrainment rate of the cavity or the cavity volume change as a function of the cavity length or cavitation number. The general equation for a ventilated cavity with vaporization and diffusion may be written

$$\dot{M}_{VG} + \dot{M}_{DG} + \dot{M}_V - \dot{M}_E = \frac{d}{dt}(\rho_c \overline{V}) \tag{5}$$

where $\dot{M}_{VG}$ = Mass flow rate of ventilated gas into cavity,

$\dot{M}_{DG}$ = Mass flow rate of diffused gas into cavity,

$\dot{M}_V$ = Mass flow rate of vapor into cavity,

$\dot{M}_E$ = Mass flow rate of the entrained vapor and gas out of cavity,

ρ_c = Mass density of vapor-gas mixture in the cavity,

$\overline{V}$ = Cavity volume.

Clearly, contributions due to each term in Equation (5) have to be

investigated separately to obtain a thorough analysis.

For a water entry, obviously $\dot{M}_{VG} = 0$. If, in addition, diffusion and vaporization can be neglected during the process, then the equation will simplify to $\dot{M}_E = -\frac{d}{dt}(\rho_c V)$.

For a steady flow in the absence of diffusion and vaporization, $\dot{M}_E = \dot{M}_{VG}$.

The coefficient C_Q is shown as a function of cavitation number for velocities of 30, 45, and 50 ft/sec in Figures 11 - 14. These results show the same qualitative trends as those of Billet and Weir (1974) on ogive head forms, namely, that C_Q increases as velocity and/or cavity length increase. Billet and Weir assumed that C_Q was a function of R_e , F_r , and L/D and correlated their data with an equation of the form

$$C_Q \cong C\, R_e^{\,m}\, F_r^{\,n}\, (L/D)^p \qquad (6)$$

where R_e and F_r are the Reynolds number and Froude number, respectively, based on the model diameter. The exponents m, n, p and the constant C were determined for their experiment from the best curve fit through the experimental data, and had the values $C = 0.424 \times 10^{-2}$, $m = 0.21$, $n = 0.07$, $p = 0.7$ for the zero caliber ogive and $C = 0.32 \times 10^{-4}$, $m = 0.52$, $n = 0.37$, $p = 0.6$ for the quarter caliber ogive.

They also developed a theoretical method which can be applied to correct the experimental results if other processes such as diffusion and vaporization exist. The importance of diffusion and vaporization processes

in water entry will have to be evaluated by an analysis of Equation (5) employing the results of Billet and Weir (1974). The best curve fits for the present data are given by $C_Q = 0.164 \times 10^{-7} R_e^{0.92} F_r^{0.44} (L/D)^{0.67}$ for the 18° conical head models and $C_Q = 0.595 \times 10^{-4} R_e^{0.41} F_r^{0.15} (L/D)^{0.81}$ for the 45° conical head models. From Figures 11 - 14 it is seen that C_Q increases as the body becomes blunt, i.e., the 45° conical head model gives a higher value of C_Q than the 18° conical head model for a given model diameter and cavity length. Also, for a given body shape, C_Q increases as the size of the model and/or the velocity increase. All these tendencies are in agreement with the results by Billet and Weir (1974) on ogive head forms.

3.3 Cavity Area Coefficient

When analyzing the diffusion and vaporization at the cavity wall, it will be necessary to know the surface area of the cavity. The area can be expressed in dimensionless form as the cavity area coefficient, C_A, defined as

$$C_A = \frac{A}{D^2} \tag{7}$$

where A is the cavity surface area and D the model diameter. The cavity surface area was determined by the procedure developed by Billet (1970) and Billet, Holl and Weir (1974) in which the cavity shape as determined from photographs of the cavity is approximated by an ellipsoid. The cavity area coefficient is shown as a function of L/D in Figures 15 and 16, and as one would expect C_A increases as the body becomes more

blunt for the given value of L/D, i.e., as the cone angle increases. The data in Figures 15 and 16 are correlated in the form $C_A = 3.32\ (L/D)^{1.09}$ for the 18° cone and $C_A = 3.55\ (L/D)^{1.17}$ for the 45° cone.

3.4 Pressure Distribution on the 45° Conical Model

The pressure distribution on the 1-inch diameter 45° conical model was measured for various cavitation numbers and velocities. The pressure was expressed in dimensionless form as the pressure coefficient, C_p, defined by

$$C_p = \frac{P-P_\infty}{\frac{1}{2}\rho V_\infty^2} \tag{8}$$

where P is the pressure on the model surface. The primary purpose of these tests was to compare the pressure distribution for a ventilated cavity with the earlier results of Rouse and McNown (1948) for vaporous cavities.

In Figures 17 - 21, the pressure coefficient is shown as a function of dimensionless distance along the body surface, S/D, for velocities of 30, 45, and 50 ft/sec for values of L/D from 0 to 5. Also, for comparison purposes, the earlier results of Rouse and McNown (1948) are shown in Figures 18 and 19. However, the comparisons are better seen in Figures 20 and 21 where less data are shown.

In Figure 20, the results are compared with those of Rouse and McNown for a cavitation number of $\sigma = 0.374$. Note that the data of Rouse and McNown are interpolated values. The agreement is excellent except at the tap position 7 ($S/D \cong 1.25$), where a moderate discrepancy between the two results is shown. This may be due to the fact that near tap

position 7 the slope of the pressure distribution is so steep that any slight change in the tap location on the model due to machining or other causes will create an enormous difference in the measured pressure coefficient. Since tap position 7 on the model may not have been precisely the same as on the model used by Rouse and McNown, it is possible that a slight deviation in the tap position may be responsible for this apparent discrepancy. At other tap positions where the C_p slope is rather gradual, this behavior would not happen and the agreement is shown to be very satisfactory.

Another comparison between the present data and those of Rouse and McNown are shown in Figure 21. Note that the cavitation numbers for the two cases are slightly different ($\sigma = 0.51$ for the present data and $\sigma = 0.5$ for those of Rouse and McNown). One again observes a large discrepancy between the two results at tap position 7, as expected from the previous argument. Also observed is a drastic difference between the two results at tap position 9. This is due to the following fact: In the present case, the cavitation number $\sigma = 0.51$ corresponds to $L/D = \frac{1}{2}$ which in turn corresponds almost precisely to tap position 9. That is, in the present measurements, the cavity terminates at pressure tap 9 or perhaps the pressure tap was even outside the cavity, in which case the pressure tap would experience a pressure which is much higher than the cavity pressure. On the other hand, for the data of Rouse and McNown σ was 0.5, which will give a cavity terminus point slightly behind tap position 9 so that the tap will register the cavity pressure. However, even in their case, the C_p value at tap position 9 is slightly

higher than that of tap position 8 because tap position 9 is still very close to the cavity terminus point and may have been influenced by it. In case of a longer cavity where all the taps are positioned sufficiently inside the cavity, this behavior would not be expected as clearly demonstrated in Figure 20 for L/D = 1.

Rouse and McNown did not specify either the velocities or the model diameters for their data, but the range of velocities for their experiment was 10 ft/sec to 35 ft/sec.

3.5 Cavity Attrition Test

The cavity decay test was conducted according to the procedure described in Section 2. The results obtained from this test are shown in Figure 22 - 27. For an unsteady flow, one may have two kinds of instantaneous cavitation numbers, each of them defined by

$$\sigma_t = \frac{P_\infty(t)-P_c(t)}{\frac{1}{2}\rho V_\infty^2(t)} \tag{9}$$

and

$$\sigma_P = \frac{P_\infty(t)-P_c(t)}{P_o(t)-P_\infty(t)} \tag{10}$$

respectively. Here, $P_\infty(t)$ and $V_\infty(t)$ are the instantaneous pressure and velocity at the test section, $P_c(t)$ is the instantaneous cavity pressure, and $P_o(t)$ is the instantaneous pressure at the tunnel stagnation section. Note that $P_o-P_\infty = \frac{1}{2}\rho V_\infty^2$ for a steady flow, assuming V_o, the velocity at the stagnation section, is small. $P_o(t)-P_\infty(t)$, $P_\infty(t)$, $P_c(t)$ were

all measured during the test. However, $V_\infty(t)$ was not directly measured during the test and so it was necessary to calculate $V_\infty(t)$ from the data for $P_o(t)-P_\infty(t)$. It can be shown that $\frac{1}{2}\rho V_\infty^2 > P_o(t)-P_\infty(t)$ for a decelerating flow as in the present case. This can be seen by writing the unsteady Bernoulli equation along the center streamline of the tunnel in the form

$$\int_{x_o}^{x_\infty} \frac{\partial V}{\partial t}\, dx + \frac{V_\infty^2(t)}{2} + \frac{P_\infty(t)}{\rho} = \frac{P_o(t)}{\rho} + \frac{V_o^2(t)}{2} \tag{11}$$

Here, subscripts ∞ and o denote the tunnel test section and the stagnation section, respectively. For a decelerating flow, $\frac{\partial V}{\partial t} < 0$ and therefore one must have $\frac{1}{2}\rho V_\infty^2(t) > P_o(t)-P_\infty(t)$ so that $\sigma_t < \sigma_p$.

The procedure of obtaining $V_\infty(t)$ from the measured values of $P_o(t)-P_\infty(t)$ is explained in the following:

The unsteady Bernoulli equation along the center streamline is

$$\frac{\partial \phi}{\partial t} + \frac{1}{2}V^2(t) + \frac{P(t)}{\rho} = C(t) \tag{12}$$

where ϕ is the velocity potential and C(t) the time dependent constant of integration. Assuming the velocity is fairly constant across the tunnel section, one may use a one-dimensional analysis and write

$$V_o(t)\, A_o = V(x,t)\, A(x) \tag{13}$$

where again the subscript o denotes the stagnation section of the tunnel and A(x) is the cross sectional area at x. Since $\frac{\partial \phi}{\partial x} = V(x,t)$, one obtains

$$\phi = \int_a^x V(x,t)dx + f(t) \tag{14}$$

in which a is any reference position and f(t) is a function of time only. Substituting Equations (13) and (14) into Equation (12) and relating the tunnel stagnation section and the test section, one arrives at

$$\dot{V}_o(t)A_o \int_a^{x_o} \frac{dx}{A(x)} + \frac{1}{2}V_o^2(t) + \frac{P_o(t)}{\rho} = \dot{V}_o(t)A_o \int_a^{x_\infty} \frac{dx}{A(x)} + \frac{1}{2}V_\infty^2(t) + \frac{P_\infty(t)}{\rho} \tag{15}$$

where the subscript ∞ again refers to the test section of the tunnel and the dot denotes differentiation with respect to time. In the 12-inch tunnel where this experiment was conducted, the contraction ratio for the nozzle is 3:1 which is the ratio of the stagnation section diameter to the test section diameter. Therefore, $V_\infty(t) = 9\ V_o(t)$. Thus, Equation (15) reduces to

$$C_o\dot{V}_o(t) + 40\ V_o^2(t) + \frac{P_\infty(t)-P_o(t)}{\rho} = 0 \tag{16}$$

where

$$C_o = A_o \int_{x_o}^{x_\infty} \frac{dx}{A(x)} \quad .$$

The constant C_o was calculated by numerically integrating $1/A(x)$ between the two pressure tap locations x_o and x_∞ corresponding to P_o

and P_∞ using the tunnel section drawings. This calculation gave $C_o \cong 24.15$. Therefore, Equation (16) can be rewritten

$$24.15\ V_o\ (t) + 40\ V_o^2(t) + \frac{P_\infty(t)-P_o(t)}{\rho} = 0 \quad . \tag{17}$$

Since we know the values of $P_o(t)-P_\infty(t)$ from the oscillogram tracing, this equation could be numerically integrated for $V_o(t)$ using the fourth order Runge-Kutta method.

Figure 22 shows the instantaneous cavitation number σ_t based on $\frac{1}{2}\rho V_\infty^2(t)$ thus obtained versus the instantaneous dimensionless cavity length L(t)/D. Also, steady state data taken from Figure 3 are plotted in Figure 22. The flow deceleration for the test, i.e. $\dot{V}_\infty(t)$ was approximately 3 ft/sec^2. The agreement between the unsteady data and the steady data is seen to be very good. This can be interpreted as supporting evidence that for this value of flow deceleration at least some aspects of unsteady water entry phenomenon may be studied using a quasi-steady approach to the problem. In a real water entry, the deceleration of the object varies widely depending on the size, shape, mass, impact velocity, etc. Thus it will be necessary to investigate the applicability of the quasi-steady analysis for the entire range of decelerations of practical interest. In some cases, these are greater than those of the present study.

In Figure 23 is replotted a set of data taken from Figure 22, indicating a sequence of the events in time. The time t = (N-1)/8 second, where N is the data point number in a sequential order of time,

was measured from the moment the tunnel and the ventilation air flow were shut down. The cavity length is shown to grow slightly after the shut-off for this particular set of data, and then diminishes continuously until it disappears. The entire event took place in about one second.

Figure 24 shows a comparison between the instantaneous cavitation number σ_p based on $P_o(t)-P_\infty(t)$ and σ_t based on $\frac{1}{2}\rho V_\infty^2(t)$. This set of data corresponds to the third run of Figure 22. Comparisons between σ_p and σ_t for the three test runs are tabulated in Section E of the Appendix for Cavity Attrition Test Data. The difference between the two cavitation numbers σ_p and σ_t is seen to be small in the present case because the deceleration of the flow during the test was only about 2.7 ft/sec^2 , i.e., $\dot{V}_\infty(t) \cong -2.7$ ft/sec^2 or $\dot{V}_o(t) \cong -0.3$ ft/sec^2 and therefore the first term in Equation (17) is negligibly small compared with the second term and consequently one nearly restores $\frac{1}{2}\rho V_\infty^2 \cong P_o-P_\infty$. However, if $|\dot{V}_\infty(t)|$ is moderately large, the situation will become different and one will expect a noticeable discrepancy between σ_p and σ_t.

Figures 25 - 27 show the history of $P_\infty(t)$ and $V_\infty(t)$ from the moment the tunnel was shut off. $P_\infty(t)$ was measured directly, whereas $V_\infty(t)$ was calculated from the measured data for $P_o(t)-P_\infty(t)$ in a manner already described above. In all three runs, $\dot{V}_\infty(t)$ is shown to be about -3 ft/sec^2.

[4] CONCLUSIONS AND RECOMMENDATIONS

(1) The preliminary results obtained for steady state ventilated

cavities are in good agreement with those of the earlier study for vaporous cavitation by Rouse and McNown (1948), except for the pressure distribution data at several points where the pressure can change rather abruptly.

(2) The ventilation air flow coefficient data also give the same qualitative trend as those of Billet and Weir (1974) for ogive bodies.

(3) The cavity area coefficient as a function of dimensionless cavity length also shows the same qualitative trend as that of Billet (1970) and Billet, Holl, and Weir (1974).

(4) The data obtained by the exploratory attempt for the cavity attrition test in which the deceleration was approximately 3 ft/sec^2 indicates that the instantaneous cavitation number versus the instantaneous dimensionless cavity length is in good agreement with the corresponding results for the steady state measurements. This result is supportive of a possible use of quasi-steady analysis in the water tunnel for studying at least some aspects of unsteady water entry problems for decelerations of the order of 3 ft/sec^2.

(5) It will be necessary to investigate the applicability of the quasi-steady analysis for the entire range of decelerations of practical interest.

(6) For future unsteady water entry simulation studies in the water tunnel, the following factors should be considered:

1. The instantaneous velocity at the tunnel test section should be measured directly, if this cannot be obtained

accurately from the pressures.

2. It is well known that there is an essential difference between the accelerating flow past a cavitating body at rest, which corresponds to the water tunnel situation, and an accelerating body-cavity through a fluid otherwise at rest in an inertial frame, even though the relative acceleration remains the same in both cases. This point was emphasized by Yih (1960).

[5] ACKNOWLEDGMENTS

The help of M. L. Billet was essential for the completion of the tests documented in this report. In addition, the assistance of Messrs. D. S. Weir, R. W. Woods and B. W. Henninger in conducting the tests is acknowledged.

The investigation was sponsored by the Naval Sea Systems Command and was conducted to support water entry investigation at the Naval Surface Weapons Center.

[6] REFERENCES

1. Aronson, P. M., Dawson, V. C. D., and Marks, C. H. (1974 a), "Cavity-Running Drag Coefficients of Water-Entry Bodies," ASME Cavitation and Polyphase Flow Forum -- 1974.

2. Aronson, P. M., and Marks, C. H. (1974 b), "Minimum Pressure Scaling in Water-Entry Cavities," ASME Cavitation and Polyphase Flow Forum -- 1974.

3. Baldwin, J. (1972), "An Experimental Investiation of Water Entry," Ph. D. Thesis, University of Maryland.

4. Billet, M. L. (1970), "Thermodynamic Effects on Developed Cavitation in Water and Freon 113," M.S. Thesis, Pennsylvania State University.

5. Billet, M. L., Holl, J. W. and Weir, D. S. (1974), "Geometric

Description of Developed Cavities in Zero and Quarter Caliber Ogive Bodies," Applied Research Laboratory, Technical Memorandum 74 - 136, 6 May 1974.

6. Billet, M. L., and Weir, D. S. (1974), "The Effect of Gas Diffusion and Vaporization on the Entrainment Coefficient for a Ventilated Cavity," Applied Research Laboratory Technical Memorandum 74 - 15.

7. May, A. (1972), "Water Entry," Alden Research Laboratories Report No. 115 - 72/SP, Holden, Massachusetts.

8. Rouse, H. and McNown, J. S. (1948), "Cavitation and Pressure Distribution, Head Forms at Zero Angle of Yaw," Studies in Engineering Bulletin 32, State University of Iowa.

9. Waugh, J. G., and Stubstad, G. W. (1972), Hydroballistics Modeling, Naval Undersea Center, San Diego, California.

10. Yih, C-S. (1960), "Finite Two-Dimensional Cavities," Proc. Royal Society (London), A258, 90-100.

June 18, 1975
JHK:JWH:jep

APPENDIX -- TABULATION OF EXPERIMENTAL DATA

The list of the experimental data is given in the following tables. Each data point represents an average of several runs. For model descriptions, see Section 2.

June 18, 1975
JHK:JWH:jep

A. L/D vs. σ

Model I: 45° cone angle x $\frac{1}{2}$ inch diameter

L/D	σ(cavitation number)		
	V_∞=30 fps	V_∞=45 fps	V_∞=50 fps
1	0.353	0.328	0.359
2	0.250	0.231	0.244
4	0.152	0.159	0.161
8	0.095	0.105	0.109
10	0.087	0.094	0.102

Model II: 45° cone angle x 1 inch diameter

L/D	σ(cavitation number)		
	V_∞=30 fps	V_∞=45 fps	V_∞=50 fps
1/2	0.510	0.512	0.523
1	0.374	0.379	0.372
2	0.254	0.251	0.267
4	0.189		
5	0.179		

June 18, 1975
JHK:JWH:jep

Model III: 18° cone angle x $\frac{1}{2}$ inch diameter

L/D	σ(cavitation number)		
	V_∞=30 fps	V_∞=45 fps	V_∞=50 fps
1	0.186	0.182	0.186
2	0.138	0.131	0.140
4	0.098	0.099	0.101
8	0.073	0.066	0.074
10	0.063	0.062	0.065

Model IV: 18° cone angle x 1 inch diameter

L/D	σ(cavitation number)		
	V_∞=30 fps	V_∞=45 fps	V_∞=50 fps
1/2	0.249	0.229	0.230
1	0.174	0.185	0.191
2	0.141	0.146	0.147
4	0.103	0.115	0.113
5	0.095	0.103	0.111

June 18, 1975
JHK:JWH:jep

B. σ vs. C_Q

Pair = pressure at the flowmeter in psig

P_c = cavity pressure in transducer volts (transducer slope = 5.886 psi/volt)

P_∞ = ambient pressure in transducer volts (transducer slope = 5.886 psi/volt)

Q = ventilation air flow rate in ft^3/sec

C_Q = ventilation air flow coefficient, $\frac{Q}{V_\infty D^2}$

Model I: 45° cone angle x $\frac{1}{2}$ inch diameter

V_∞=30 fps

Q(cfs)	Pair(psig)	P_∞(volt)	P_c(volt)	σ	C_Q
0.00071	5	0.798	0.411	0.3773	0.0137
0.00126	6	0.673	0.429	0.2371	0.0244
0.00205	10	0.568	0.404	0.1596	0.0395
0.00246	12	0.532	0.4265	0.1022	0.0474
0.00257	12	0.508	0.4125	0.0925	0.0495

June 18, 1975
JHK:JWH:jep

V_∞=45 fps

Q(cfs)	Pair(psig)	P_∞(volt)	P_c(volt)	σ	C_Q
0.00129	9	1.441	0.632	0.3503	0.0165
0.00251	15	1.108	0.552	0.2407	0.0322
0.00434	27	0.891	0.500	0.1693	0.0557
0.00612	42	0.740	0.497	0.1052	0.0784
0.00653	44	0.720	0.493	0.0982	0.0837

V_∞=50 fps

Q(cfs)	Pair(psig)	P_∞(volt)	P_c(volt)	σ	C_Q
0.00154	12	1.828	0.822	0.3525	0.0178
0.00277	18	1.450	0.752	0.2446	0.0319
0.00533	39	1.185	0.739	0.1563	0.0615
0.00730	55	1.029	0.717	0.1093	0.0842
0.00777	59	1.003	0.713	0.1016	0.0896

June 18, 1975
JHK:JWH:jep

Model II: 45° cone angle x 1 inch diameter

V_∞=30 fps

Q(cfs)	Pair(psig)	P_∞(volt)	P_c(volt)	σ	C_Q
0.00151	4	0.804	0.295	0.4956	0.0073
0.00348	12	0.691	0.321	0.3602	0.0167
0.00762	37	0.670	0.429	0.2346	0.0366
0.01269	67	0.605	0.412	0.1879	0.0610
0.01456	78	0.640	0.430	0.2044	0.0700

V_∞=45 fps

Q(cfs)	Pair(psig)	P_∞(volt)	P_c(volt)	σ	C_Q
0.00252	9	1.601	0.423	0.51	0.0081
0.00615	28	0.283	0.403	0.381	0.0197
0.01254	63	0.939	0.350	0.255	0.0402

V_∞=50 fps

Q(cfs)	Pair(psig)	P_∞(volt)	P_c(volt)	σ	C_Q
0.00282	12	2.056	0.543	0.5302	0.0081
0.00712	36	1.564	0.507	0.3704	0.0205
0.01450	79	1.302	0.577	0.2540	0.0418

Model III: 18° cone angle x $\frac{1}{2}$ inch diameter

V_∞=30 fps

Q(cfs)	Pair(psig)	P_∞(volt)	P_c(volt)	σ	C_Q
0.00023	1	0.388	0.201	0.182	0.0045
0.00031	2	0.332	0.202	0.1265	0.0060
0.00043	2	0.295	0.188	0.1041	0.0083
0.00049	2	0.290	0.221	0.0671	0.0095
0.00058	2.5	0.274	0.196	0.0759	0.0113

V_∞=45 fps

Q(cfs)	Pair(psig)	P_∞(volt)	P_c(volt)	σ	C_Q
0.00062	0	0.2	-0.213	0.1788	0.0080
0.00085	0	0.074	-0.234	0.1333	0.0110
0.00113	0	0.043	-0.192	0.1017	0.0145
0.00161	2	0	-0.16	0.0692	0.0207
0.00191	4	0.076	-0.071	0.0636	0.0245

V_∞=50 fps

Q(cfs)	Pair(psig)	P_∞(volt)	P_c(volt)	σ	C_Q
0.00070	2	0.729	0.189	0.1892	0.0081
0.00097	3	0.578	0.181	0.1391	0.0112
0.00137	3.5	0.493	0.211	0.0988	0.0159
0.00222	8	0.490	0.282	0.0728	0.0257
0.00293	12	0.490	0.306	0.0644	0.0338

Model IV: 18° cone angle x 1 inch diameter

V_∞=30 fps

Q(cfs)	Pair(psig)	P_∞(volt)	P_c(volt)	σ	C_Q
0.00090	4	0.615	0.361	0.2473	0.0043
0.00124	5	0.566	0.391	0.1704	0.0060
0.00192	8	0.537	0.389	0.1441	0.0092
0.00300	13.5	0.700	0.593	0.1041	0.0144
0.00396	20	0.696	0.601	0.0925	0.0190

V_∞=45 fps

Q(cfs)	Pair(psig)	P_∞(volt)	P_c(volt)	σ	C_Q
0.00203	4	0.448	-0.098	0.2364	0.0065
0.00246	6	0.386	-0.043	0.1857	0.0079
0.00406	18	0.612	0.269	0.1485	0.0130
0.00708	38	0.707	0.448	0.1121	0.0227
0.01334	82	0.864	0.615	0.1078	0.0427

V_∞=50 fps

Q(cfs)	Pair(psig)	P_∞(volt)	P_c(volt)	σ	C_Q
0.00095	5	1.031	0.409	0.2179	0.0028
0.00249	10	0.820	0.275	0.1910	0.0072
0.00621	37	1.161	0.678	0.1692	0.0179
0.01203	78	1.081	0.741	0.1191	0.0347
0.01291	74	0.756	0.425	0.1160	0.0372

C. Cavity Geometry

The following data for L_M , D_M , C_A and etc. were measured from the photographs.

D_M = Maximum diameter of cavity (See Figures 9 and 10)

L_M = Twice the distance between the cavity separation point and the point where the cavity diameter becomes the maximum (D_M) (See Figure 10 for definition)

Y = Radial distance from the axis of the cylindrical model to the cavity terminus. This information is necessary in calculating the cavity surface area.

C_A = Cavity area coefficient defined by A/D^2, where A is the cavity surface area and D is the model diameter

Model I: (45° cone angle x $\frac{1}{2}$ inch diameter), V_∞=45 ft/sec

L/D	L/D_M	L_M/D_M	2Y/D	C_A	σ
1	0.833	1.160	1.16	3.618	0.328
2	1.493	1.972	1.30	7.905	0.231
4	2.597	3.084	1.32	17.754	0.159
8	4.081	4.628	1.60	43.883	0.105
10	4.762	5.320	2.00	58.311	0.094

Model II: (45° cone angle x 1 inch diameter), V_∞=30 ft/sec

L/D	L/D_M	L_M/D_M	2Y/D	C_A	σ
1/2	0.459	0.482	1.08	1.689	0.510
1	0.870	1.078	1.08	3.493	0.374
2	1.538	1.648	1.10	7.658	0.254
4	2.667	2.796	1.06	17.021	0.189
5	2.913	3.496	1.10	22.255	0.179

Model III: (18° cone angle x $\frac{1}{2}$ inch diameter), V_∞=45 ft/sec

L/D	L/D_M	L_M/D_M	2Y/D	C_A	σ
1	0.906	1.120	1.014	3.388	0.182
2	1.745	1.904	1.124	6.964	0.131
4	3.200	3.200	1.144	14.951	0.099
8	5.519	6.080	1.252	33.096	0.066
10	6.40	7.440	1.252	44.730	0.062

Model IV: (18° cone angle x 1 inch diameter), V_∞=45 ft/sec

L/D	L/D_M	L_M/D_M	2Y/D	C_A	σ
1/2	0.479	0.646	1.014	1.620	0.229
1	0.931	0.980	1.044	3.315	0.185
2	1.787	1.834	1.044	6.831	0.146
4	3.309	3.576	1.074	14.471	0.115
5	3.941	4.176	1.074	18.744	0.103

D. Pressure Distribution on Model II (45° Cone Angle x $\frac{1}{2}$ inch Diameter)

See Figures 17 - 21 for the location of the pressure taps. In the following tables,

June 18, 1975
JHK:JWH:jep

$$C_{P_i} = \frac{P_i - P_\infty}{\frac{1}{2}\rho V_\infty^2}, \quad i=1,2,\ldots,9$$

where i denotes the pressure tap number.

V_∞=30 ft/sec

C_{P_i} \ L/D	0	$\frac{1}{2}$	1	2	4	5
C_{P_1}	0.3784	0.3809	0.3850	0.3926	0.4042	0.4067
C_{P_2}	0.2683	0.2736	0.2807	0.2936	0.3094	0.3128
C_{P_3}	0.2014	0.2092	0.2192	0.2345	0.2549	0.2588
C_{P_4}	0.1348	0.1467	0.1608	0.1815	0.2077	0.2114
C_{P_5}	0.0530	0.0725	0.0934	0.1211	0.1523	0.1591
C_{P_6}	-0.0827	-0.0411	-0.0054	0.0351	0.0749	0.0881
C_{P_7}	-0.4972	-0.3437	-0.2491	-0.1630	-0.0963	-0.0735
C_{P_8}	-0.1423	-0.4290	-0.3792	-0.2500	-0.1620	-0.1304
C_{P_9}	-0.0983	-0.0584	-0.3709	-0.2501	-0.1606	-0.1315

June 18, 1975
JHK:JWH:jep

V_∞=45 ft/sec

C_{P_i} \ L/D	0	$\frac{1}{2}$	1	2
C_{P_1}	0.3725	0.3826	0.3870	0.3956
C_{P_2}	0.2645	0.2767	0.2823	0.2953
C_{P_3}	0.1994	0.2123	0.2214	0.2387
C_{P_4}	0.1347	0.1505	0.1634	0.1872
C_{P_5}	0.0516	0.0752	0.0956	0.1241
C_{P_6}	-0.0866	-0.0385	-0.0026	0.0402
C_{P_7}	-0.5335	-0.3372	-0.2430	-0.1544
C_{P_8}	-0.1492	-0.4479	-0.3826	-0.2564
C_{P_9}	-0.0990	-0.0757	-0.3718	-0.2555

V_∞=50 ft/sec

C_{P_i} \ L/D	0	$\frac{1}{2}$	1	2
C_{P_1}	0.3740	0.3768	0.3821	0.3905
C_{P_2}	0.2652	0.2711	0.2784	0.2903
C_{P_3}	0.1977	0.2080	0.2192	0.2343
C_{P_4}	0.1283	0.1460	0.1615	0.1828
C_{P_5}	0.0490	0.0711	0.0935	0.1208
C_{P_6}	-0.0890	-0.0420	-0.0039	0.0361
C_{P_7}	-0.5556	-0.3415	-0.2427	-0.1572
C_{P_8}	-0.1504	-0.4423	-0.3821	-0.2613
C_{P_9}	-0.1000	-0.0322	-0.3726	-0.2606

E. Cavity Attrition Test Data

$$\sigma_P = \frac{P_\infty(t)-P_c(t)}{P_o(t)-P_\infty(t)} = \text{Instantaneous Cavitation Number Based on } P_o(t)-P_\infty(t)$$

$$\sigma_t = \frac{P_\infty(t)-P_c(t)}{\frac{1}{2}\rho V_\infty^2(t)} = \text{Instantaneous Cavitation Number based on } 1/2\rho V_\infty^2(t)$$

June 18, 1975
JHK:JWH:jep

First Run

t(sec)	L(t)/D	σ_p	σ_t
0	2.960	0.2236	0.2208
1/8	3.226	0.2186	0.2157
2/8	3.060	0.2245	0.2214
3/8	2.993	0.2221	0.2187
4/8	2.026	0.2562	0.2515
5/8	1.560	0.3084	0.3025
6/8	1.060	0.3654	0.3582
7/8	0.926	0.4499	0.4395
8/8	0.293	0.5070	0.4940
9/8	0.160	0.5759	0.5617

Second Run

t(sec)	L(t)/D	σ_p	σ_t
0	2.926	0.2397	0.2367
1/8	3.426	0.2274	0.2248
2/8	3.293	0.2376	0.2347
3/8	2.560	0.2516	0.2480
4/8	1.826	0.3046	0.2998
5/8	1.460	0.3222	0.3169
6/8	1.226	0.3799	0.3725
7/8	0.893	0.4386	0.4304
8/8	0.726	0.5104	0.4987
9/8	0.293	0.5781	0.5633

Third Run

t(sec)	L(t)/D	σ_p	σ_t
0	4.560	0.1864	0.1841
1/8	3.226	0.2122	0.2096
2/8	2.393	0.2569	0.2535
3/8	1.760	0.3224	0.3174
4/8	1.360	0.3829	0.3770
5/8	1.026	0.4502	0.4420
6/8	0.926	0.5069	0.4962
7/8	0.526	0.5737	0.5620

June 18, 1975
JHK:JWH:jep

LIST OF FIGURE CAPTIONS

Figure 1 - Sketch of Test Arrangement for Steady State Measurements

Figure 2 - Sketch of Test Arrangement for Cavity Attrition Tests

Figure 3 - Photograph Showing a Steady State Ventilated Cavity for 45° Conical Head Model. (Model Diameter = 1-inch, V_∞ = 45 ft/sec, L/D = 2)

Figure 4 - Photograph Showing a Steady State Ventilated Cavity for 18° Conical Head Model. (Model Diameter = 1-inch, V_∞ = 45 ft/sec, L/D = 4)

Figure 5 - Cavitation Number Versus Cavity Length for 0.5-inch Diameter, 18° Conical Head Model

Figure 6 - Cavitation Number Versus Cavity Length for 1-inch Diameter, 18° Conical Head Model

Figure 7 - Cavitation Number Versus Cavity Length for 0.5-inch Diameter, 45° Conical Head Model

Figure 8 - Cavitation Number Versus Cavity Length for 1-inch Diameter, 45° Conical Head Model

Figure 9 - Cavitation Number Versus L/D_M (All Models)

Figure 10 - Cavitation Number Versus L_M/D_M (All Models)

Figure 11 - Ventilation Air Flow Coefficient Versus Cavitation Number for 0.5-inch Diameter, 18° Conical Head Model

Figure 12 - Ventilation Air Flow Coefficient Versus Cavitation Number for 1-inch Diameter, 18° Conical Head Model

Figure 13 - Ventilation Air Flow Coefficient Versus Cavitation Number for 0.5-inch Diameter, 45° Conical Head Model

Figure 14 - Ventilation Air Flow Coefficient Versus Cavitation Number for 1-inch Diameter, 45° Conical Head Model

Figure 15 - Cavity Area Coefficient Versus Cavity Length for 18° Conical Head Models

Figure 16 - Cavity Area Coefficient Versus Cavity Length for 45° Conical Head Models

Figure 17 - Local Pressure Coefficient Along the Body Surface for 1-inch Diameter, 45° Conical Head Model at V_∞ = 30 ft/sec, for Various Cavitation Numbers

Figure 18 - Local Pressure Coefficient Along the Body Surface for 1-inch Diameter, 45° Conical Head Model at V_∞ = 45 ft/sec, for Various Cavitation Numbers

Figure 19 - Local Pressure Coefficient Along the Body Surface for 1-inch Diameter, 45° Conical Head Model at V_∞ = 50 ft/sec, for Various Cavitation Numbers

Figure 20 - Local Pressure Coefficient Along the Body Surface for 1-inch Diameter, 45° Conical Head, Compared with Data of Rouse and McNown (1948) for σ = 0.374

Figure 21 - Local Pressure Coefficient Along the Body Surface for 1-inch Diameter, 45° Conical Head at σ = 0.51, Compared with Data of Rouse and McNown (1948) at σ = 0.50

Figure 22 - Instantaneous Cavitation Number Versus Instantaneous Cavity Length for 1-inch Diameter, 45° Conical Head Model

June 18, 1975
JHK:JWH:jep

Figure 23 - Instantaneous Cavitation Number Versus Instantaneous Cavity Length for 1-inch Diameter, 45° Conical Head Model, Showing the Decay of Cavity as a Function of Time

Figure 24 - Comparison of Instantaneous Cavitation Number Based on $P_o(t)-P_\infty(t)$ with that Based on $\frac{1}{2}\rho V_\infty^2(t)$

Figure 25 - Transient Velocity and Pressure as a Function of Time for the Cavity Attrition Test (First Run)

Figure 26 - Transient Velocity and Pressure as a Function of Time for the Cavity Attrition Test (Second Run)

Figure 27 - Transient Velocity and Pressure as a Function of Time for the Cavity Attrition Test (Third Run)

June 18, 1975
JHK:JWH:jep

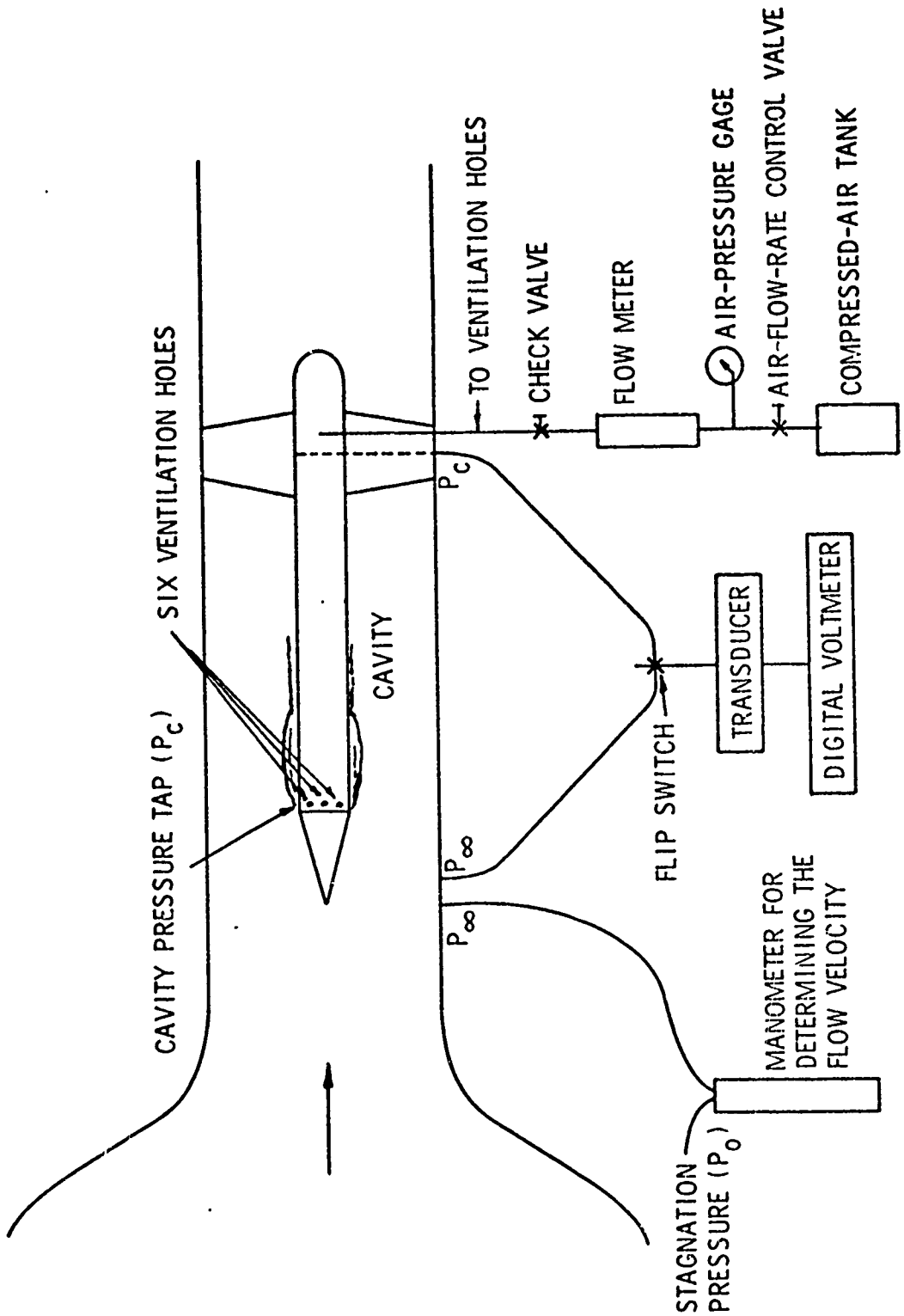

Figure 1 - Sketch of Test Arrangement for Steady State Measurements

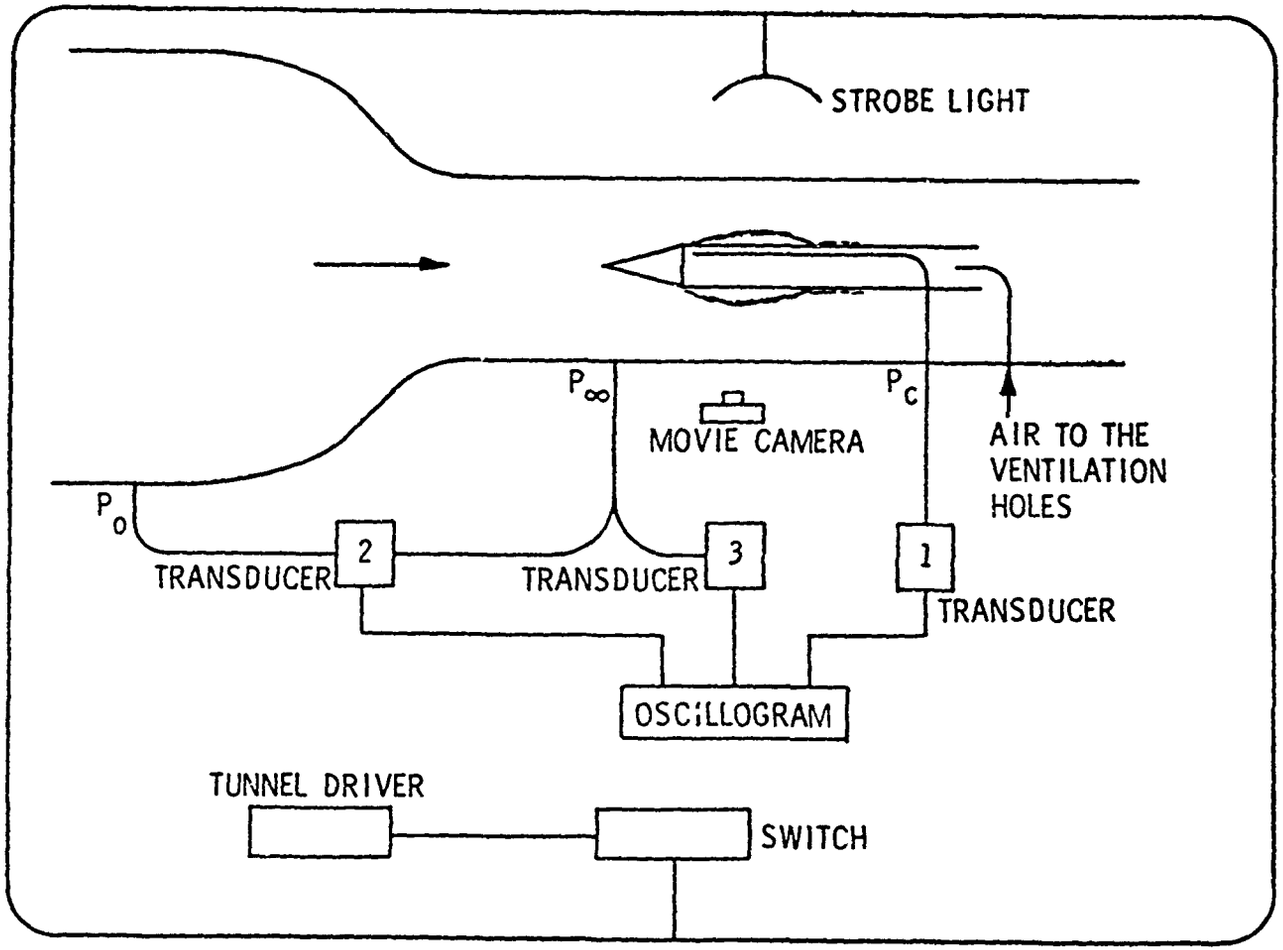

Figure 2 - Sketch of Test Arrangement for Cavity Attrition Tests

June 18, 1975
JHK:JWH:jep

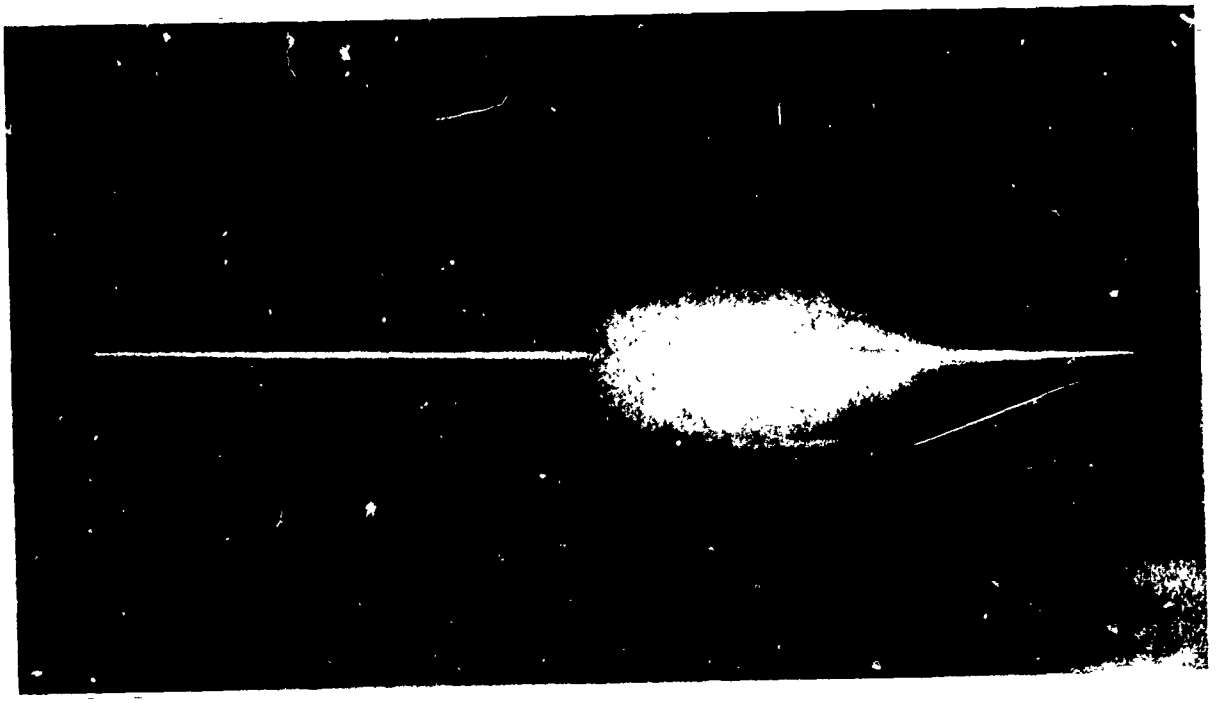

Figure 3 - Photograph Showing a Steady State Ventilated Cavity for 45° Conical Head Model. (Model Diameter = 1-inch, V_∞ = 45 ft/sec, L/D = 2)

Figure 4 - Photograph Showing a Steady State Ventilated Cavity for 18° Conical Head Model. (Model Diameter = 1-inch, V_∞ = 45 ft/sec, L/D = 4)

June 18, 1975
JHK:JWH:jep

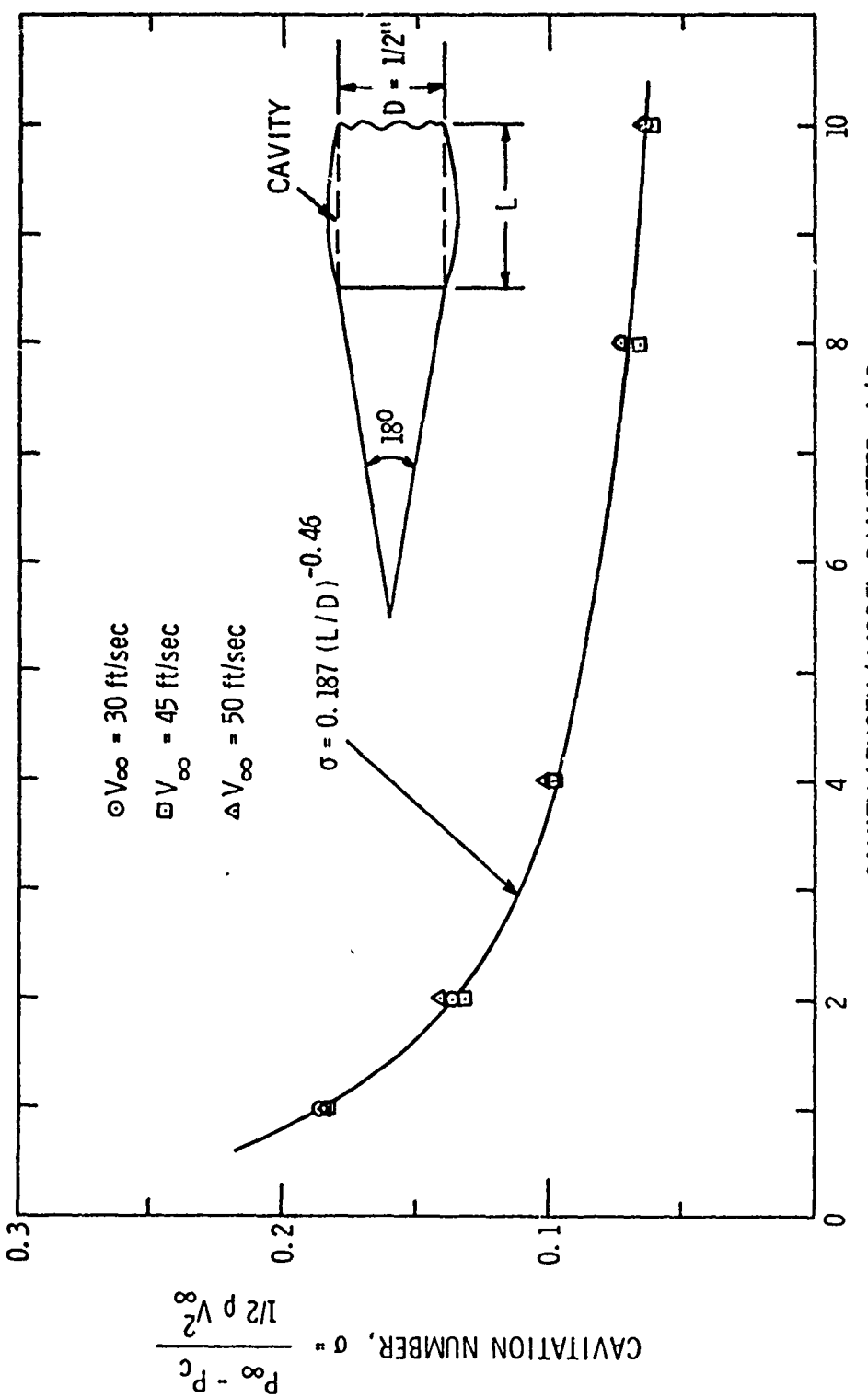

Figure 5 - Cavitation Number Versus Cavity Length for 0.5-inch Diameter, 18° Conical Head Model

June 18, 1975
JHK:JWH:jep

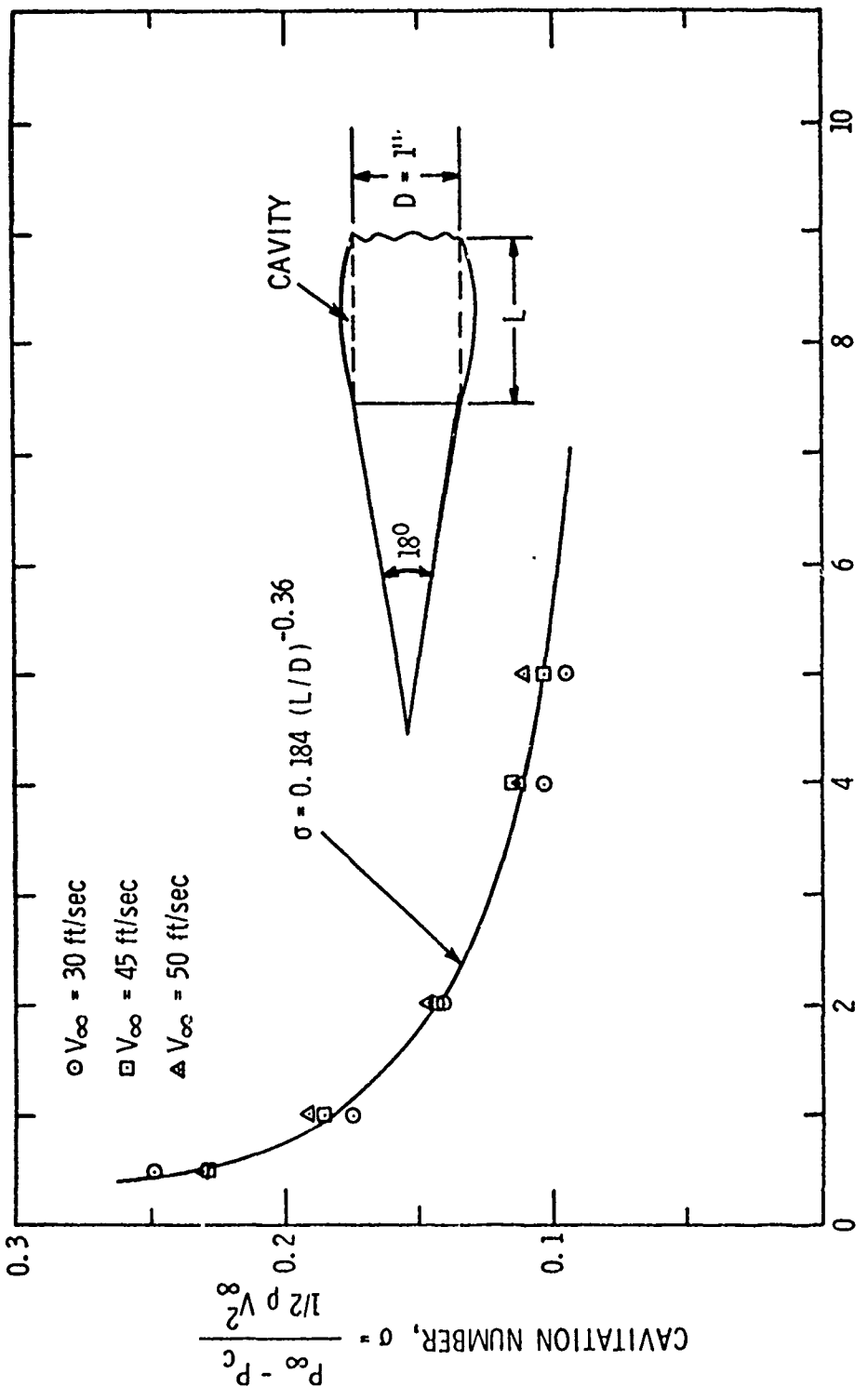

Figure 6 - Cavitation Number Versus Cavity Length for 1-inch Diameter, 18° Conical Head Model

June 18, 1975
JHK:JWH:jep

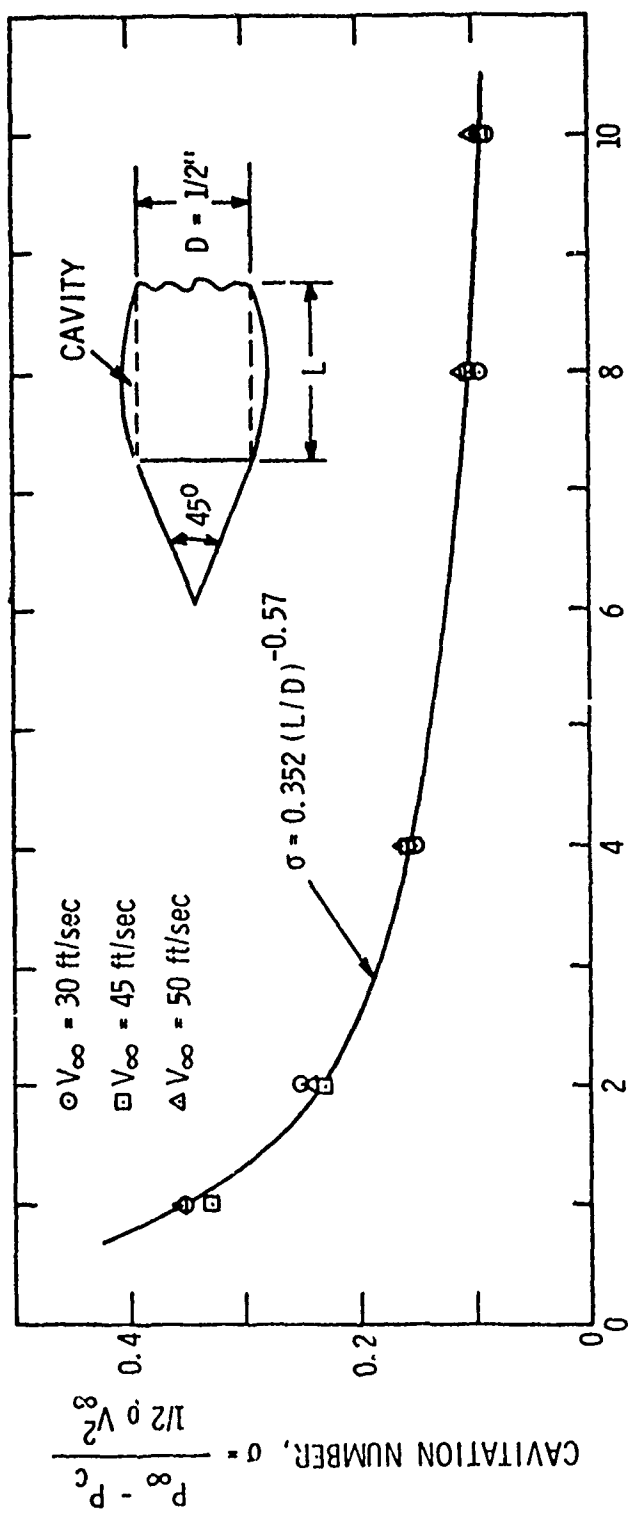

Figure 7 - Cavitation Number Versus Cavity Length for 0.5-inch Diameter, 45° Conical Head Model

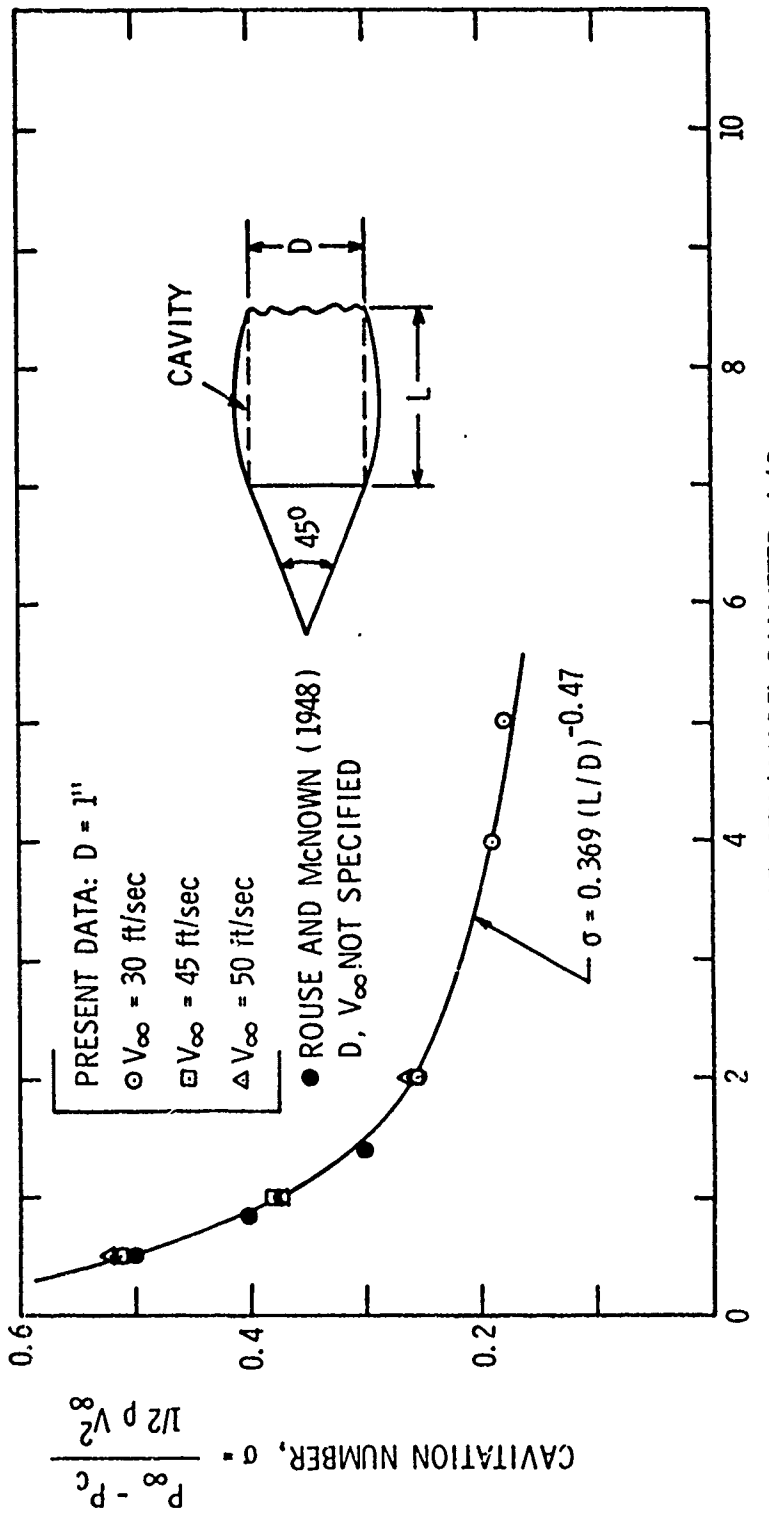

Figure 8 - Cavitation Number Versus Cavity Length for 1-inch Diameter, 45° Conical Head Model

June 18, 1975
JHK:JWH:jep

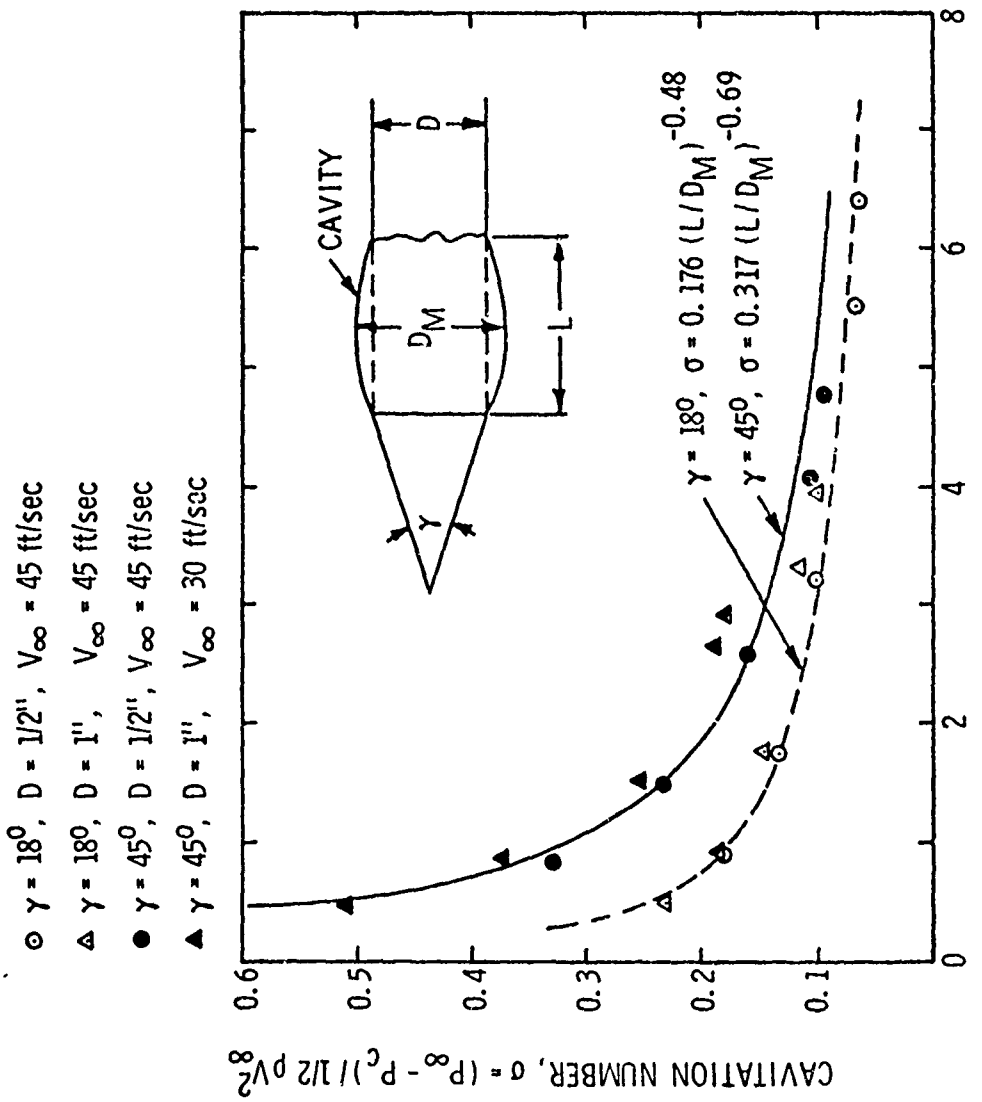

Figure 9 - Cavitation Number Versus L/D_M (All Models)

June 18, 1975
JHK:JWH:jep

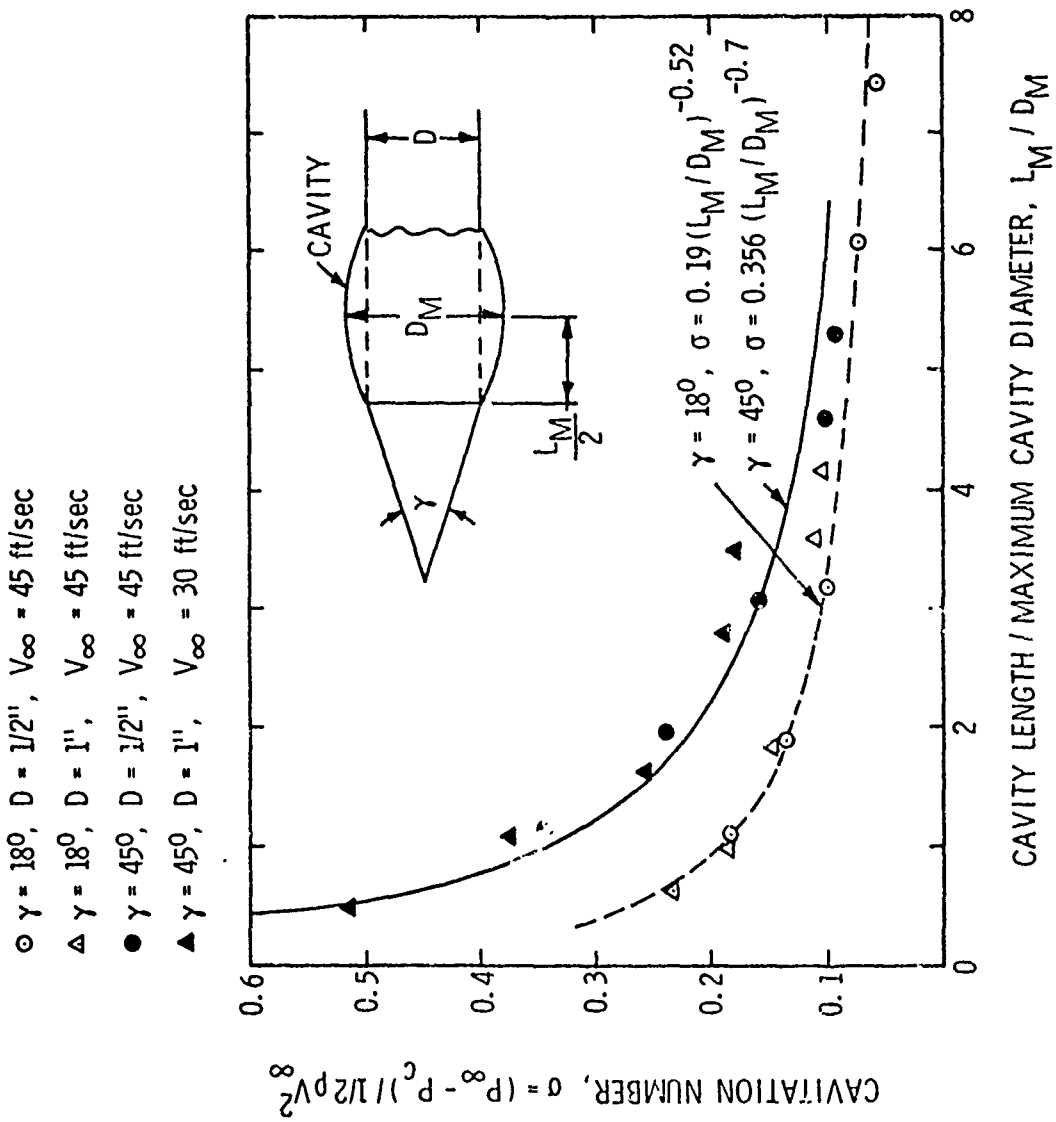

Figure 10 - Cavitation Number Versus L_M/D_M (All Models)

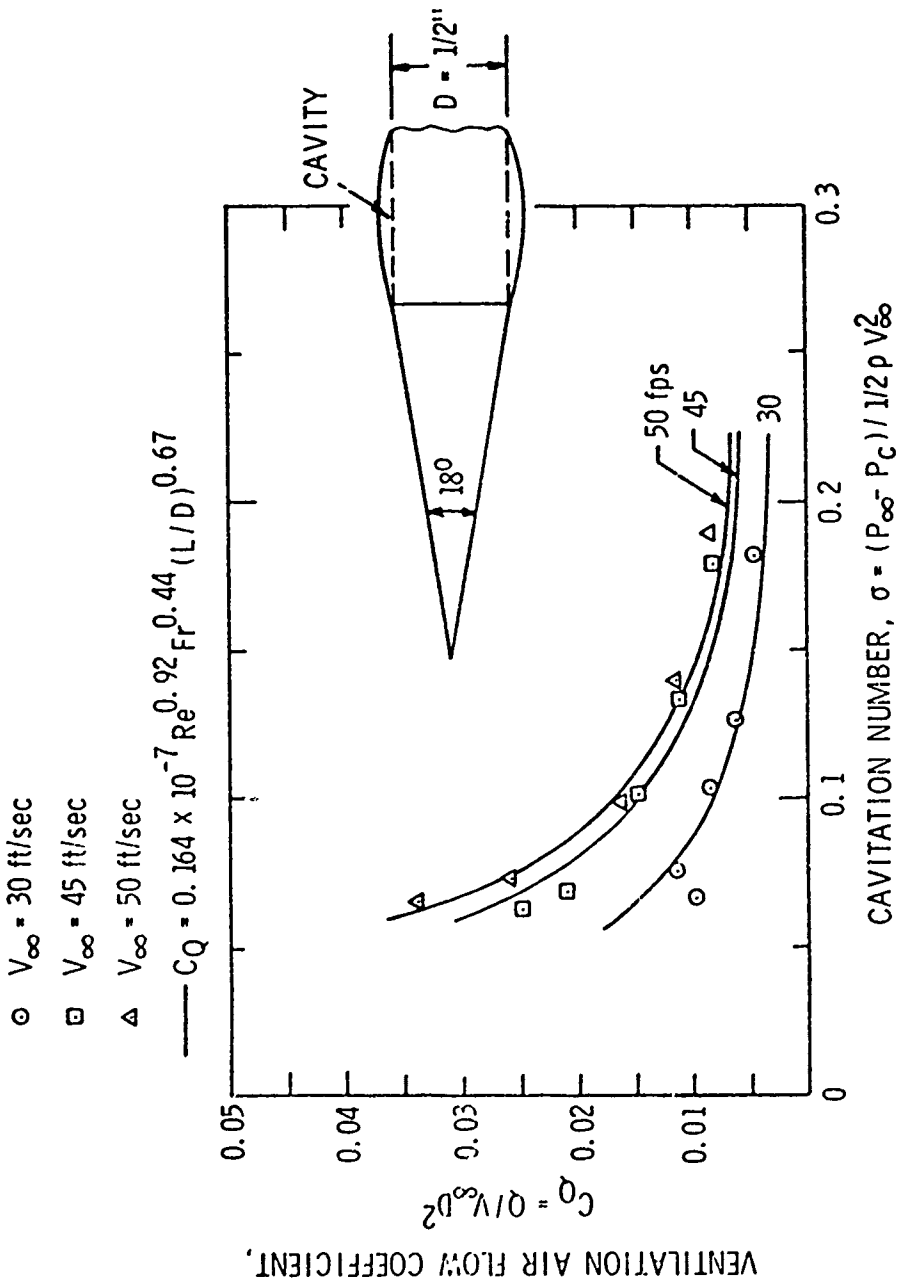

Figure 11 - Ventilation Air Flow Coefficient Versus Cavitation Number for 0.5-inch Diameter, 18° Conical Head Model

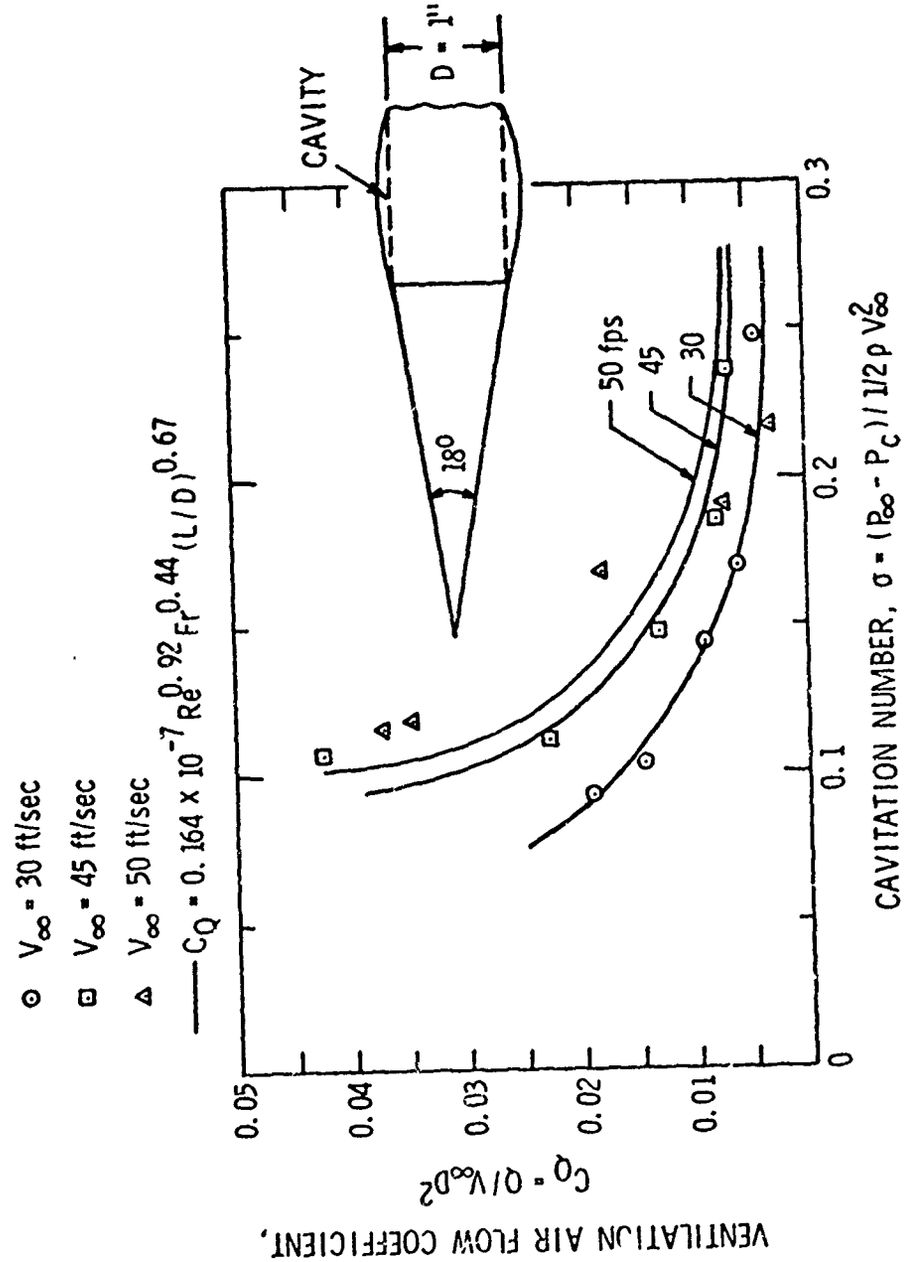

Figure 12 - Ventilation Air Flow Coefficient Versus Cavitation Number for 1-inch Diameter, 18° Conical Head Model

June 18, 1975
JHK:JWH:jep

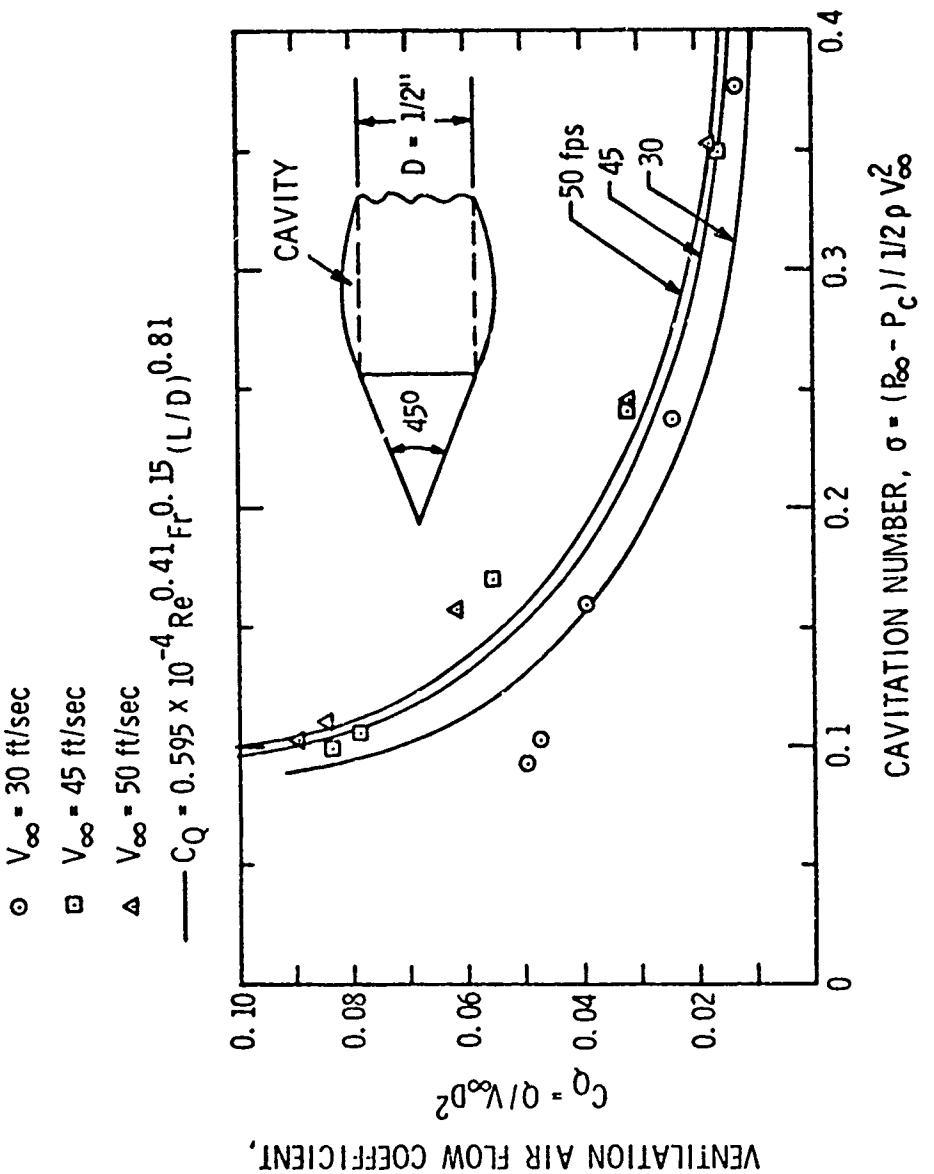

Figure 13 - Ventilation Air Flow Coefficient Versus Cavitation Number for 0.5-inch Diameter, 45° Conical Head Model

June 18, 1975
JHK:JWH:jep

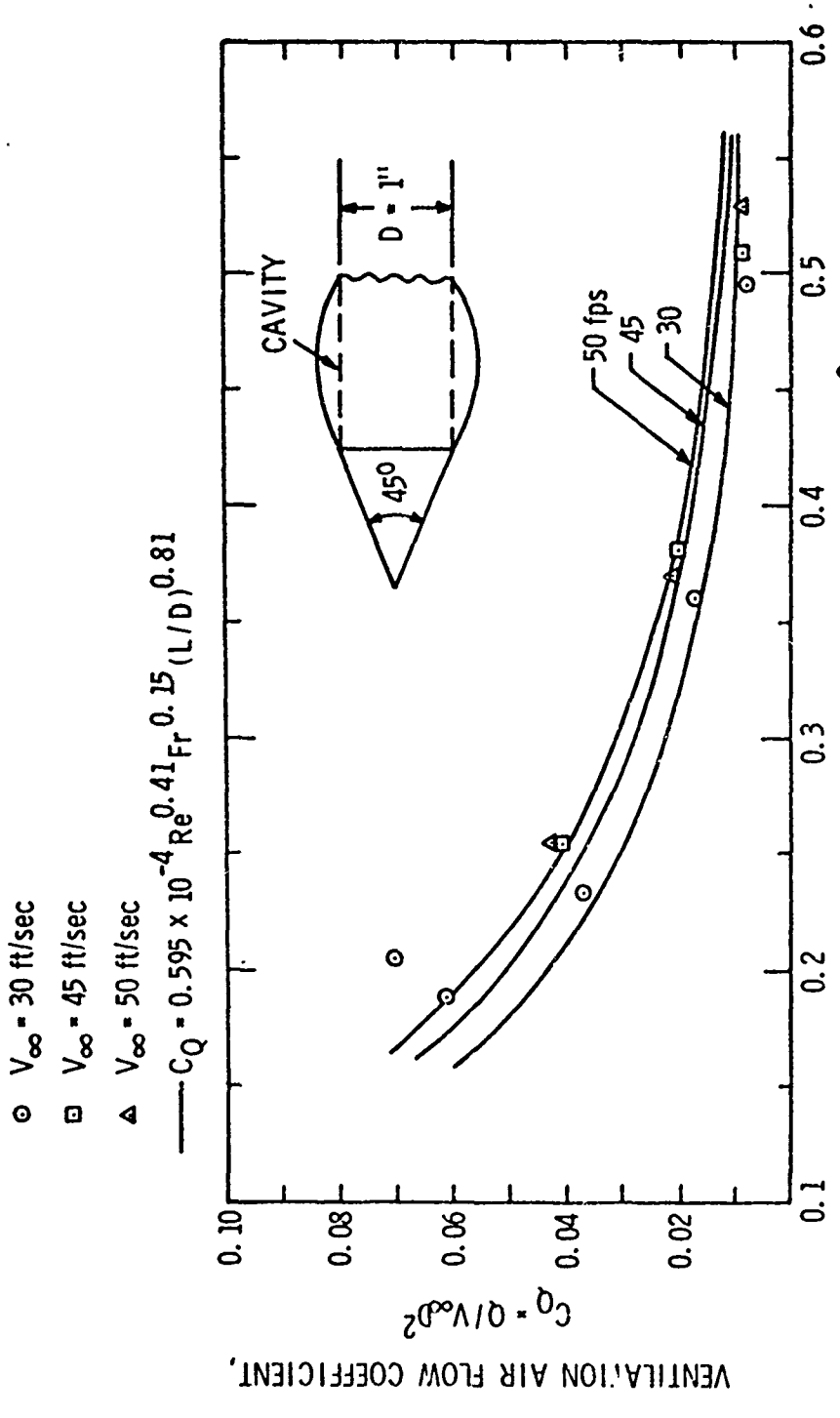

Figure 14 - Ventilation Air Flow Coefficient Versus Cavitation Number for 1-inch Diameter, 45° Conical Head Model

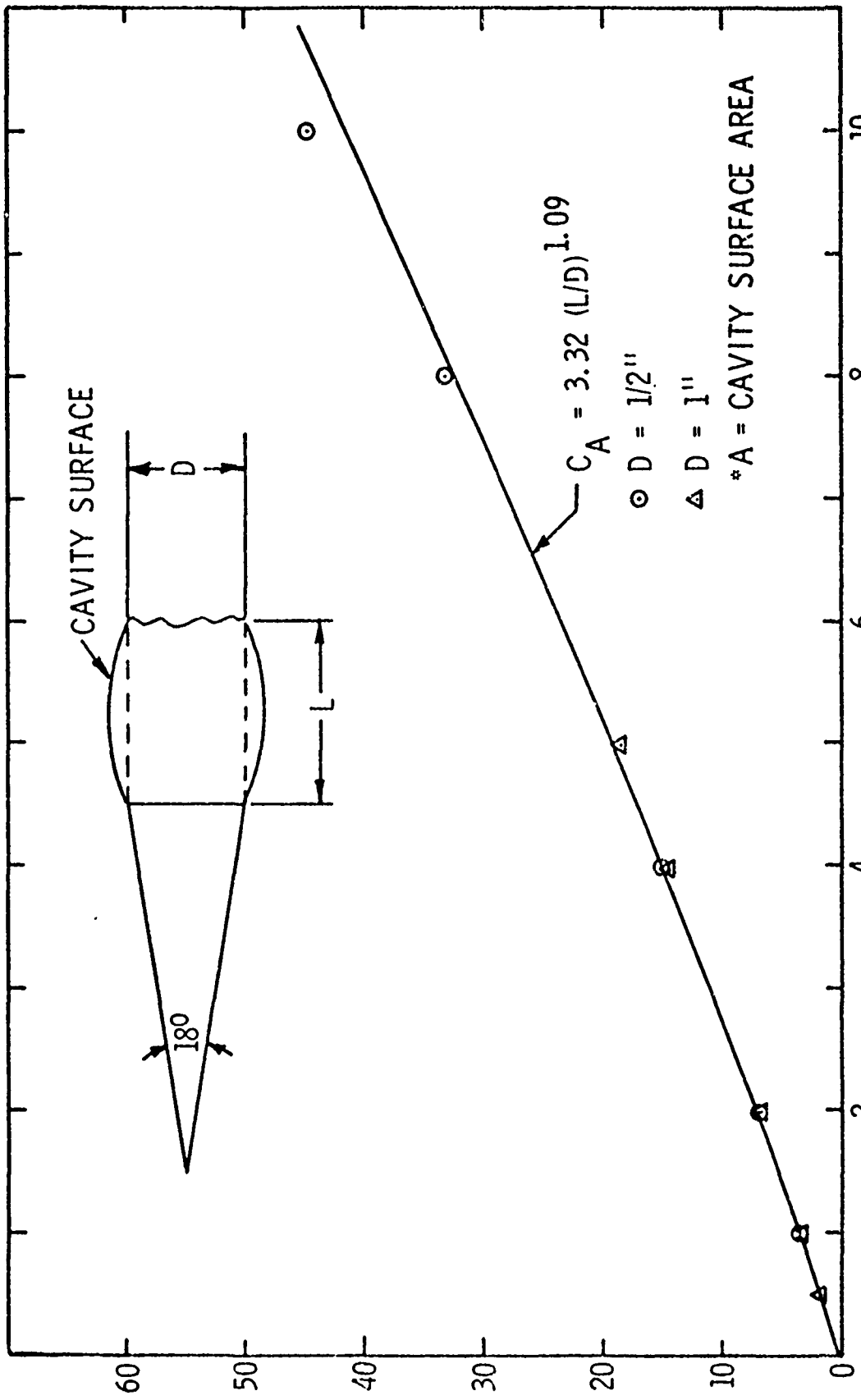

Figure 15 - Cavity Area Coefficient Versus Cavity Length for 18° Conical Head Models

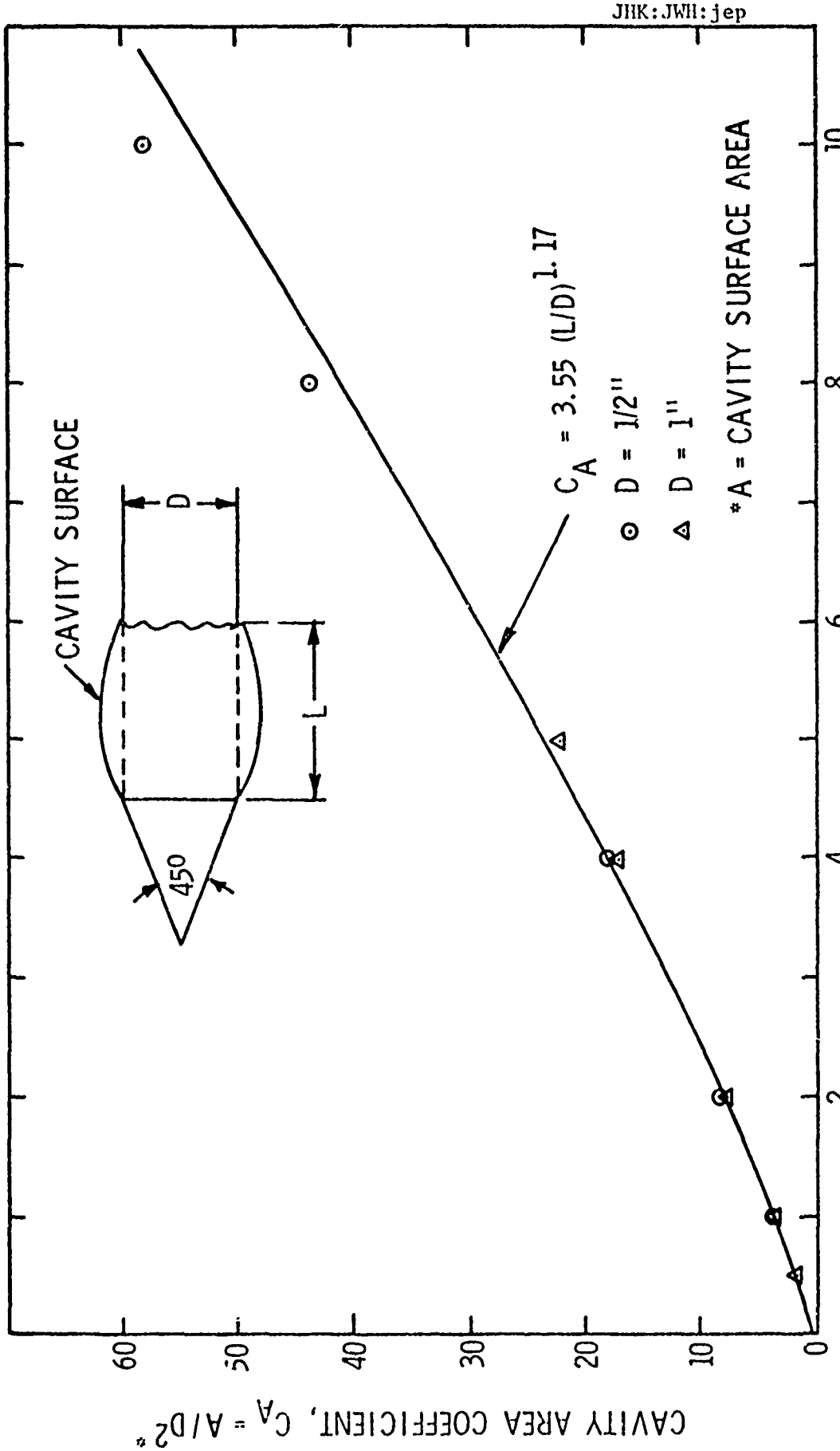

Figure 16 - Cavity Area Coefficient Versus Cavity Length for 45° Conical Head Models

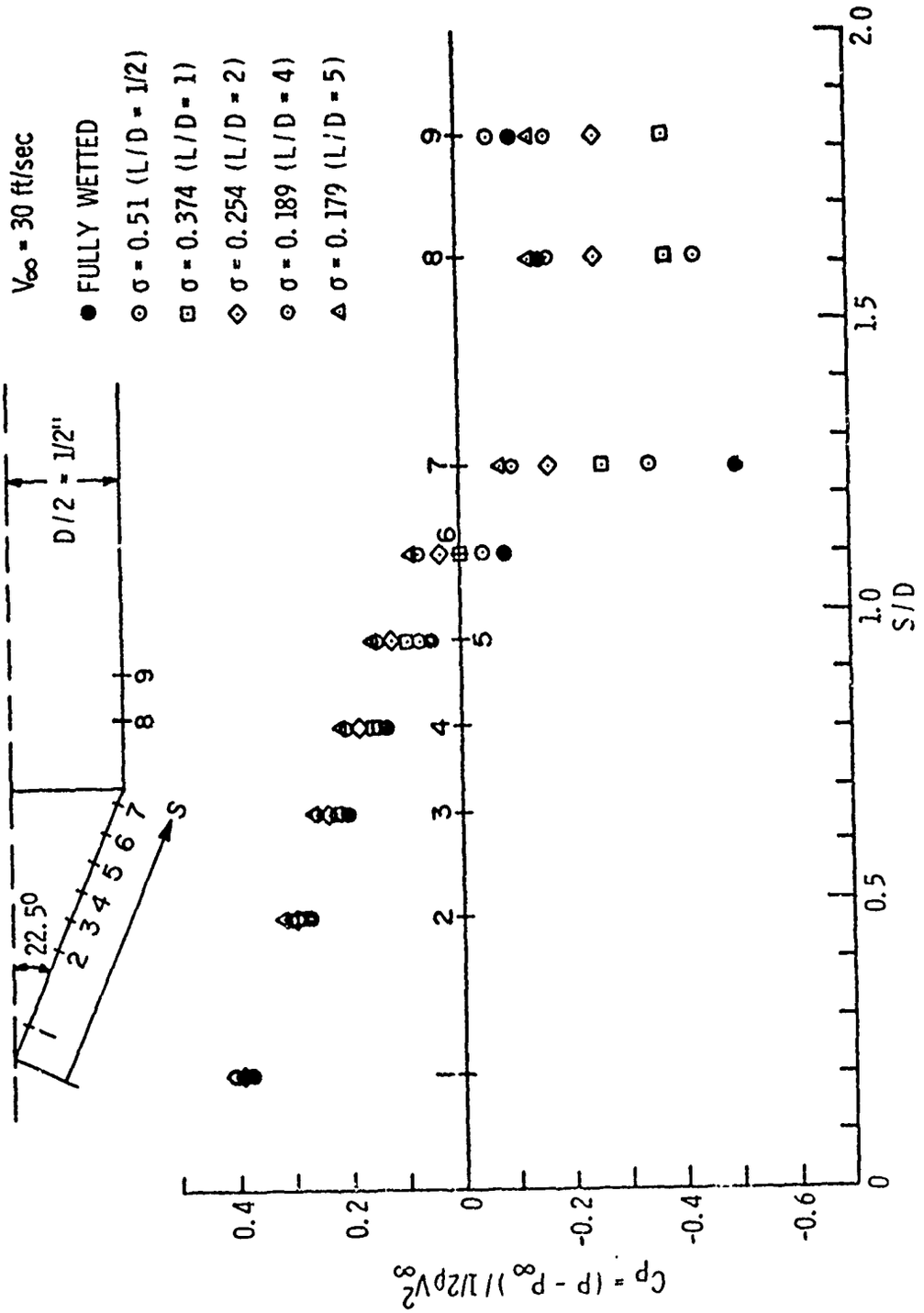

Figure 17 - Local Pressure Coefficient Along the Body Surface for 1-inch Diameter, 45° Conical Head Model at V_∞ = 30 ft/sec, for Various Cavitation Numbers

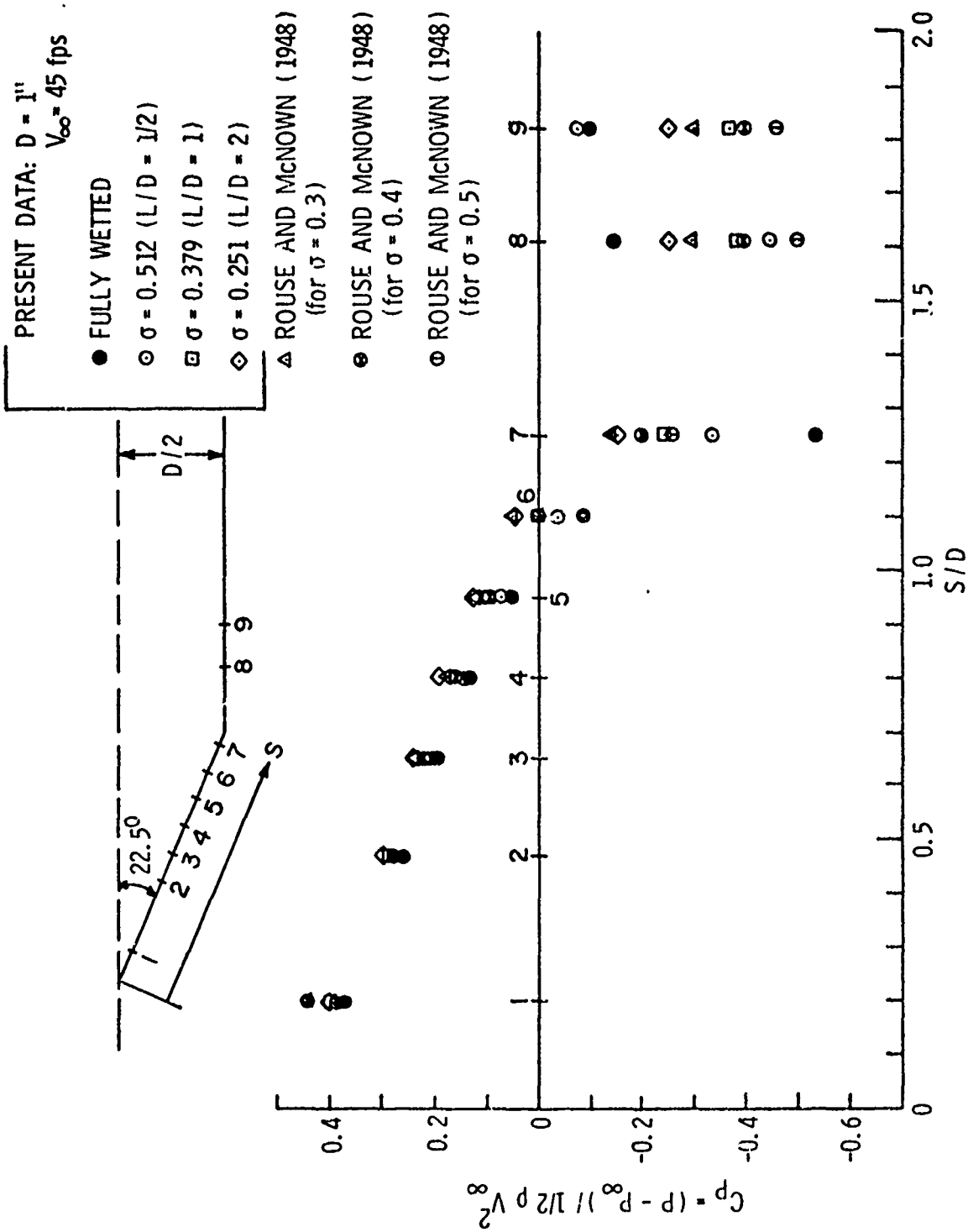

Figure 18 - Local Pressure Coefficient Along the Body Surface for 1-inch Diameter, 45° Conical Head Model at V_∞ = 45 ft/sec, for Various Cavitation Numbers

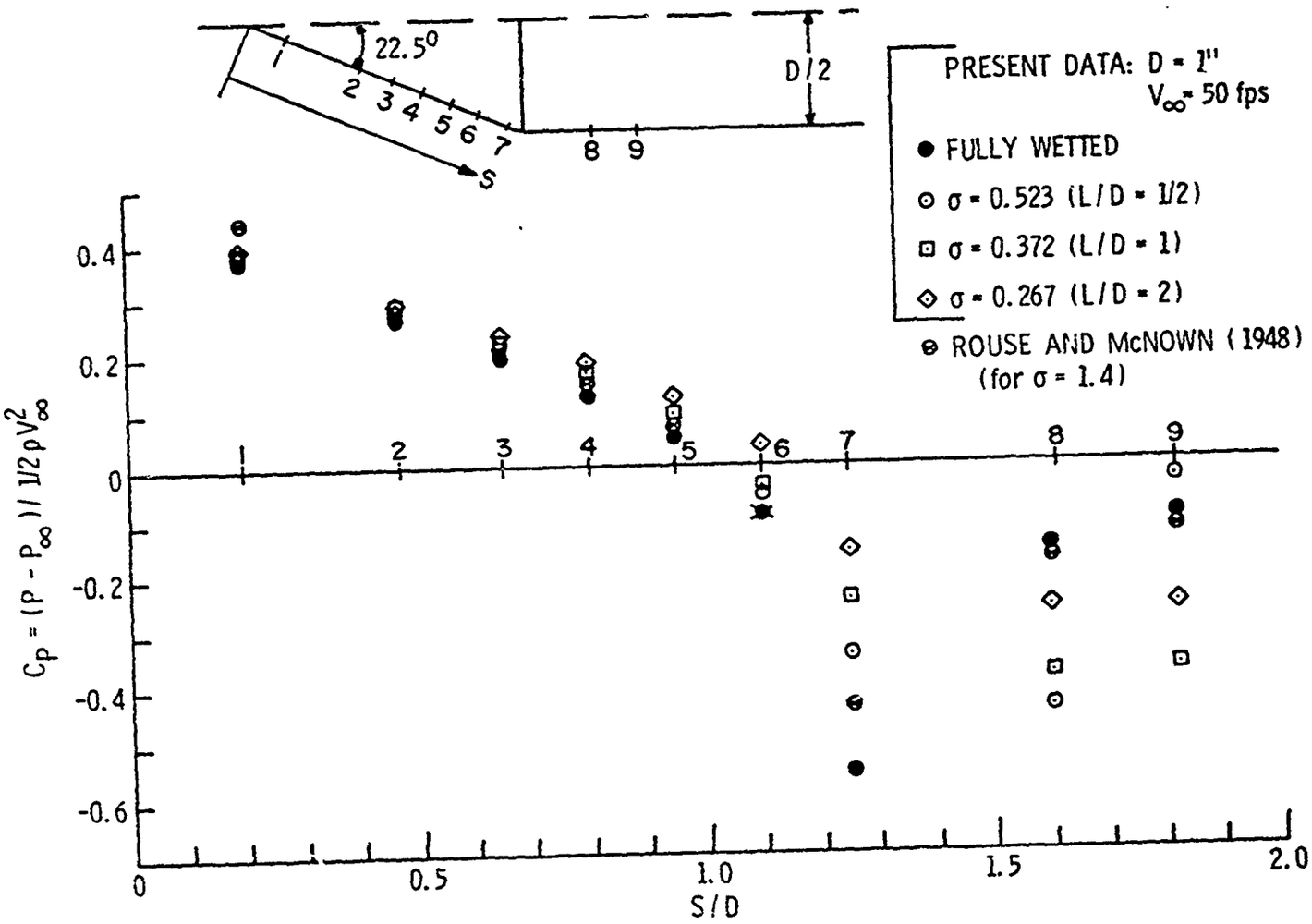

Figure 19 - Local Pressure Coefficient Along the Body Surafce for 1-inch Diameter, 45° Conical Head Model at V_∞ = 50 ft/sec, for Various Cavitation Numbers

June 18, 1975
JHK:JWH:jep

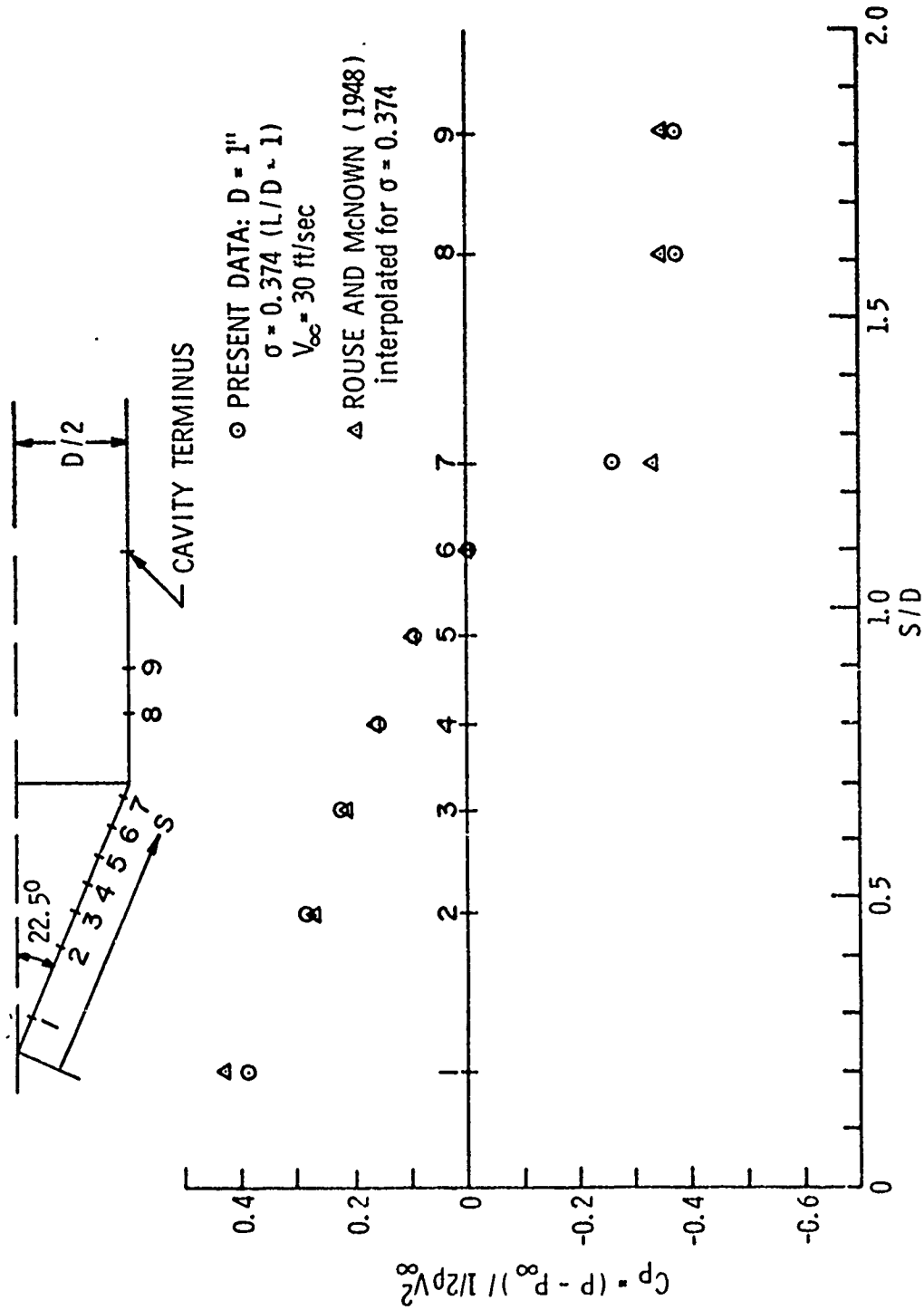

Figure 20 - Local Pressure Coefficient Along the Body Surface for 1-inch Diameter, 45° Conical Head, Compared with Data of Rouse and McNown (1948) for σ = 0.374

June 18, 1975
JHK:JWH:jep

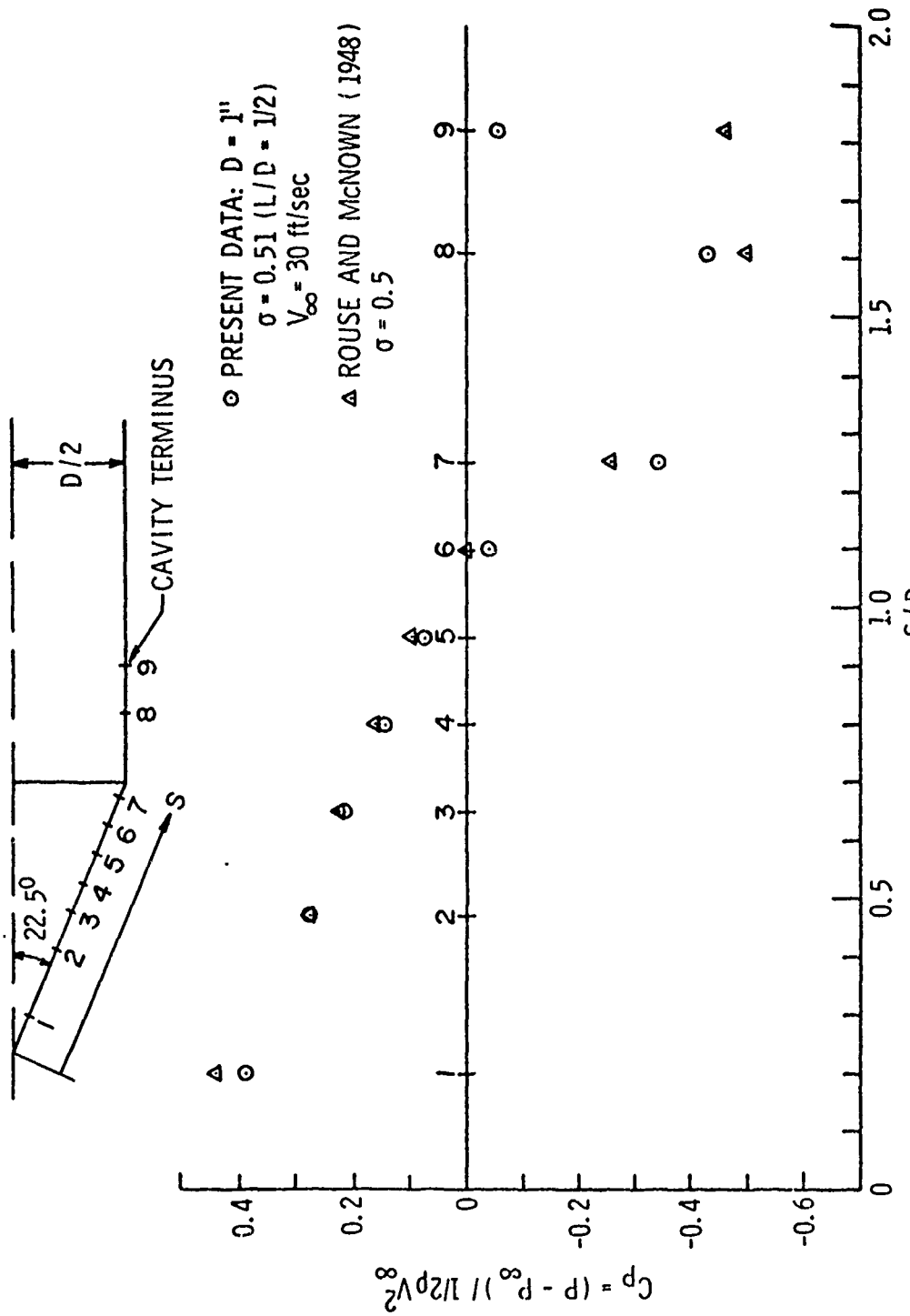

Figure 21 - Local Pressure Coefficient Along the Body Surface for 1-inch Diameter, 45° Conical Head at σ = 0.51, Compared with Data of Rouse and McNown (1948) at σ = 0.50

June 18, 1975
JHK:JWH:jep

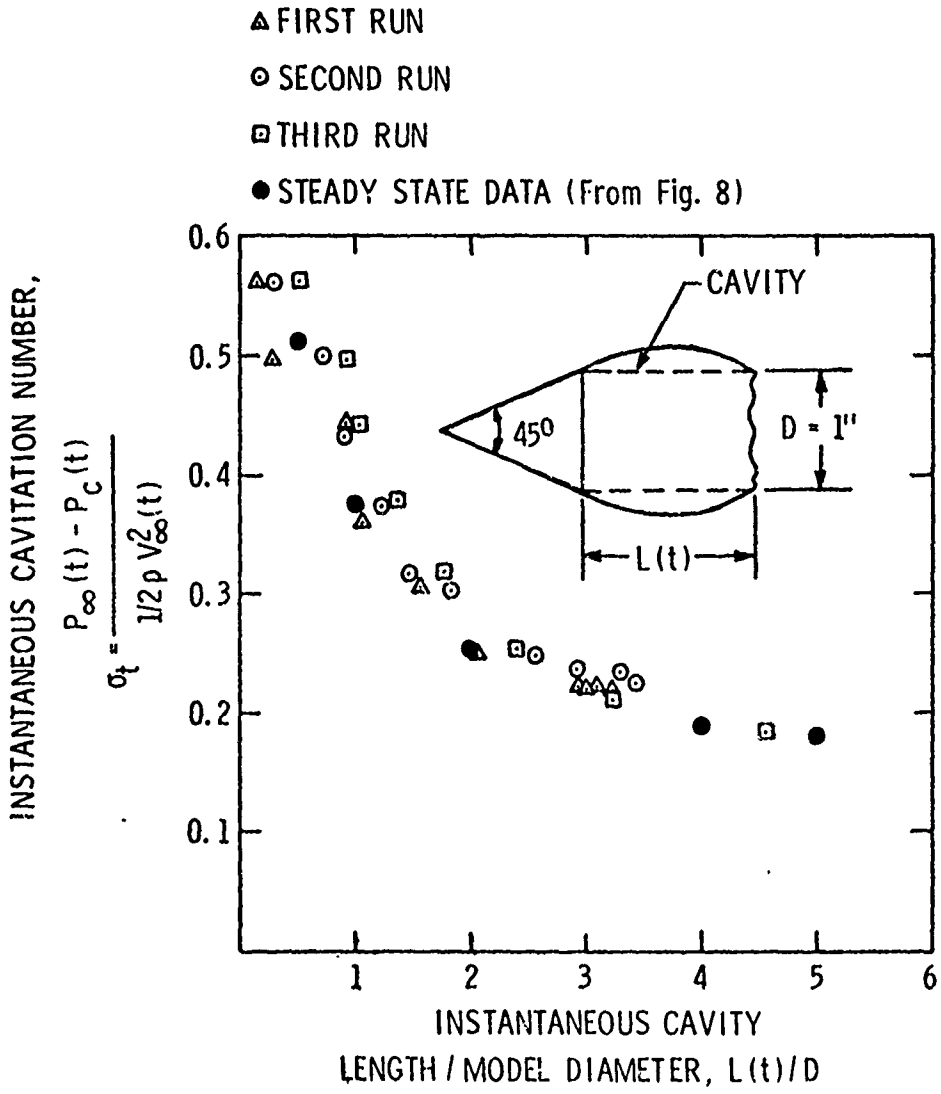

Figure 22 - Instantaneous Cavitation Number Versus Instantaneous Cavity Length for 1-inch Diameter, 45° Conical Head Model

June 18, 1975
JHK:JWH:jep

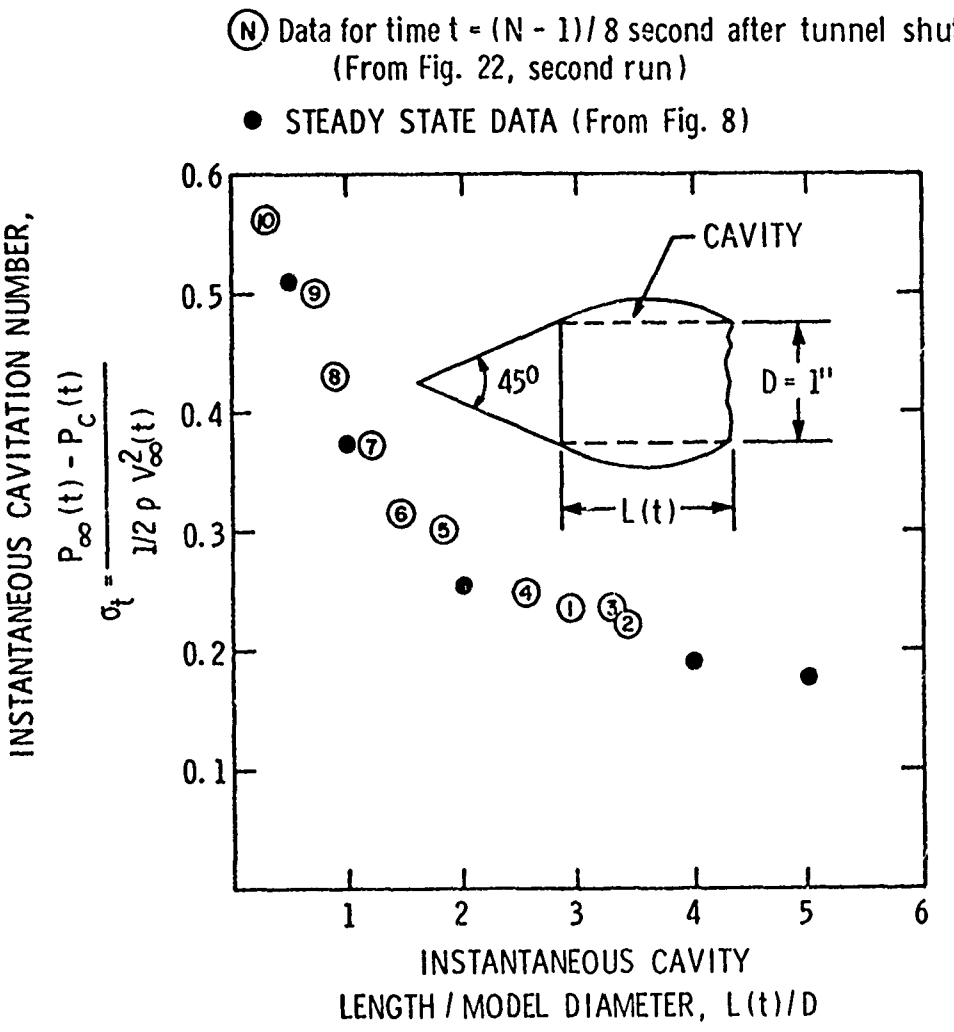

Figure 23 - Instantaneous Cavitation Number Versus Instantaneous Cavity Length for 1-inch Diameter, 45° Conical Head Model, Showing the Decay of Cavity as a Function of Time

$$\boxdot\ \sigma_t = \frac{P_\infty(t) - P_c(t)}{1/2\,\rho\, V_\infty^2(t)} \qquad \text{(From Fig. 22, third run)}$$

$$\triangle\ \sigma_p = \frac{P_\infty(t) - P_c(t)}{P_0(t) - P_\infty(t)}$$

● STEADY STATE DATA (From Fig. 8)

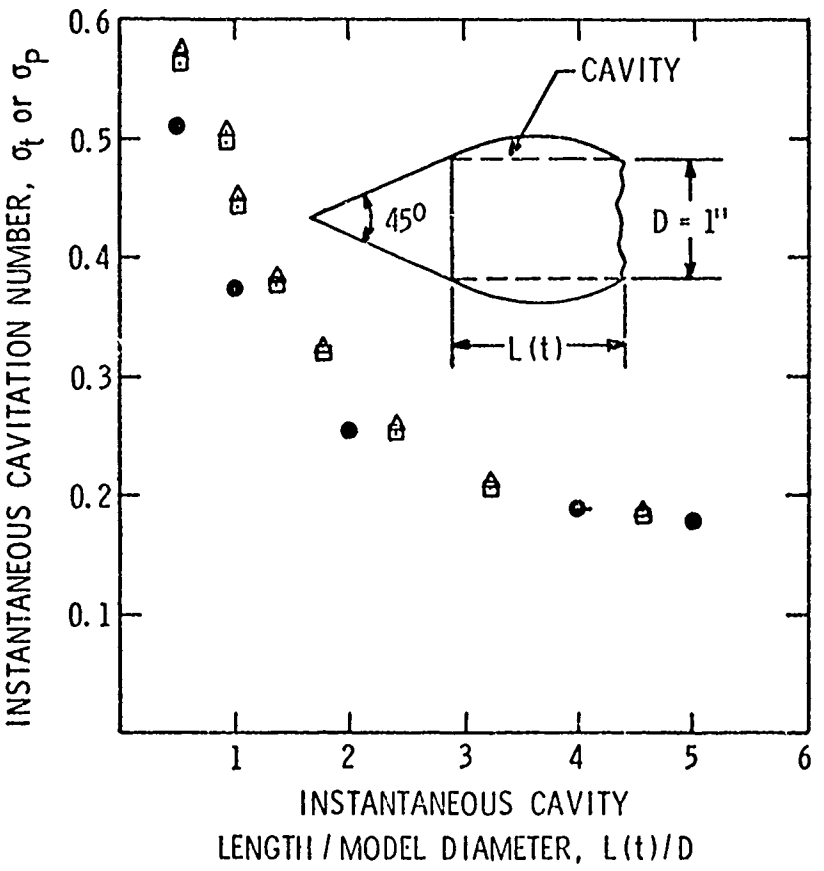

Figure 24 - Comparison of Instantaneous Cavitation Number Based on $P_0(t)-P_\infty(t)$ with that Based on $1/2\rho V_\infty^2(t)$

June 18, 1975
JHK:JWH:jep

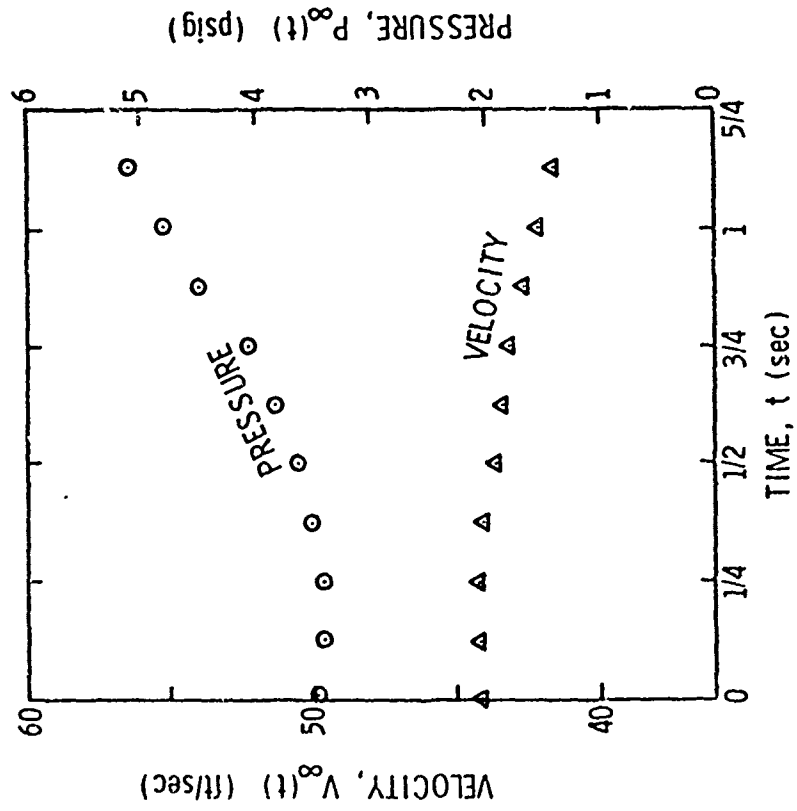

Figure 25 - Transient Velocity and Pressure as a Function of Time for the Cavity Attrition Test (First Run)

June 18, 1975
JHK:JWH:jep

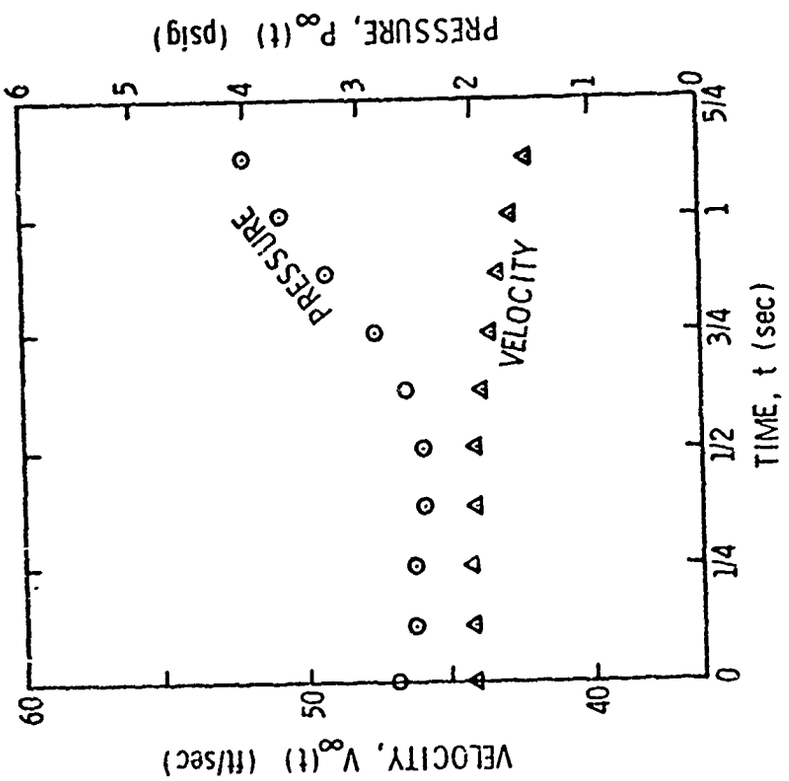

Figure 26 - Transient Velocity and Pressure as a Function of Time for the Cavity Attrition Test (Second Run)

June 18, 1975
JHK:JWH:jep

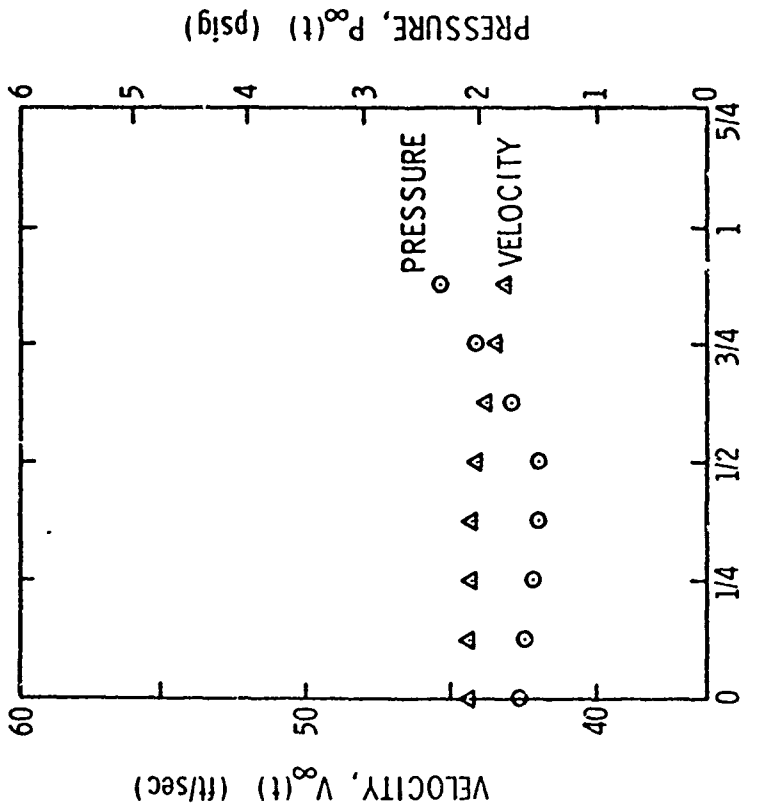

Figure 27 - Transient Velocity and Pressure as a Function of Time for the Cavity Attrition Test (Third Run)